The 1979 Nice harbour catastrophe revisited: Trigger mechanism inferred from geotechnical measurements and numerical modelling

Gabriela DAN[*1,2,] Nabil SULTAN[1], Bruno SAVOYE[1]

[1]IFREMER, Géosciences Marines, Laboratoire Environnements Sédimentaires, Plouzané, France
[2]Université de Bretagne Occidentale, IUEM, CNRS UMR6538, 29280 Plouzané, France

*: Corresponding author : Gabriela.Dan@ifremer.fr

Abstract:

In 1979, a catastrophic event occurred on the Nice continental slope (French Riviera) generating the lost of human lives and important material damages. Part of the new harbour constructed at the edge of the International Airport of Nice collapsed into the sea.

The main aim of this work was 1) to present a review of facts and details related to the 1979 accident and a review of the geological setting, and 2) to evaluate the slope stability before and after the new harbour construction, by taking into account new available data such as sediment cores and piezocone CPTU data.

The CPTU data were of great value to understand the origin of the 1979 event. They show the existence of a sensitive clay bed between 30 mbsf and 45 mbsf. Under high deviatoric load a sensitive clay layer underwent an important creep, which dramatically decreased its resistance and caused the slope failure. This working hypothesis was supported by the good agreement between the maximum thickness of the failure surface and the depth of the sensitive clay layer.

Slope stability assessment using the finite element model Femuslope show the metastable state of the Nice slope before the harbour extension. Numerical calculations demonstrated that creeping of the sensitive clay layer could be at the origin of the 1979 slide. In addition, the exceptionally heavy rainfall which occurred before the accident and consequently the seepage of fresh water probably induced the decrease of the effective stress and accelerated sediment creeping and triggered the Nice slope failure. A progressive and relatively long-term creeping failure scenario is in good agreement with the official report mentioning cracks, settlements, failures and embankment collapses occurred during land filling operations.

Keywords: Nice; 1979 event; slope stability; trigger mechanism; finite element method

1. Introduction

Submarine slope stability analyses were often carried out for a better understanding of geological phenomena which represent a risk to the coastline areas and offshore infrastructures (Locat, 2001; Locat and Lee, 2002). Occurrences of big events involving large volumes of material were identified all over the world (e.g. Storegga slide, the Canary slide) (Masson et al., 1998; Bryn et al., 2003; Haflidason et al, 2004; Canals et al., 2004). Submarine slides can generate tsunamis and affect the coastal and offshore infrastructures. The 1755 Lisbon tsunami wave represents the largest catastrophe in Western Europe, with about 60,000 casualties (Baptista et al., 1998; Canals et al., 2004). The Great Banks event (1929) following an earthquake is also an outstanding case where an initial slope failure, occurred near the earthquake epicentre, transformed into a debris flow and generated a turbidity current that cut off submarine telegraph cables (Heezen and Ewing, 1952; Piper et al., 1985; Piper et al., 1999)

Generally, a list of triggering mechanisms can be easily assessed from an accurate knowledge of the geological setting (morphology, sediment source, earthquakes, sedimentation rates, seepage, and gas hydrates…). However, the preconditions leading to failure as well as the triggering of many of the large submarine slides throughout the world is still not well understood (Lee et al., 1991; Hampton et al., 1996; Locat and Lee, 2002).

In 1979, a catastrophic slope failure accompanied by a small tsunami occurred on the Nice continental slope and generated the lost of human lives and important material damages. Part of the new harbour construction collapsed into the sea during land filling operations. The aim of the present work is 1) to present a review of facts and details related to the 1979 accident and a review of the geological setting and discuss different scenario; 2) to present new available data, such as in-situ piezocone measurements (CPTU: Cone Penetration

3

Testing) and sediment cores which provided samples for laboratory tests and 3) to evaluate the stability of the Nice slope, before and after the new harbour construction.

2. Geological context

The Var sedimentary system is located in the Ligurian Sea (NW Mediterranean) and extends from Nice coastline (SE France) to the continental slope of Corsica (**Figure 1**). During the Messinian salinity crisis, characterized by 1200 m sea-level lowering (Savoye and Piper, 1991), the Var paleo-canyon was cut on the slope (Horn et al., 1965; Clauzon, 1978; Savoye and Piper, 1991). Following the Early Pliocene transgression, the Messinian Var Valley became a ria, where Var sediments were trapped. By the Middle Pliocene, a Gilbert-type fan delta prograded to the slope break, which became the modern coastline (Clauzon et al., 1990). The Plio-Quaternary sedimentary succession deposited on the continental slope, seaward the Var delta, is 600-1000 m thick, and is formed by marls and conglomerates (Irr, 1984; Savoye et al., 1993). The Quaternary coastal uplift provides sediments supply from the glaciated Alps. Sediment on the upper slope is mainly supplied by the Var River, the Paillon River being a minor source of sediment. The two rivers are directly connected to canyons (**Figure 1**).

The continental margin offshore Nice is characterized by an absent or very narrow shelf (less than 2 km wide) (**Figure 1**). The continental slope is very steep with an average slope gradient of more than 11° (Cochonat et al., 1993). The 1000 m isobath is reached only 5 km from the coastline (Savoye et al., 1989) and the slope is locally accentuated by active erosion and gully cutting.

The Var River is located in the middle of the deltaic shelf and is prolonged in the sea by the Var Canyon (**Figure 2**). On the right side of the Var Canyon, a flat shelf is observed close to the 1979 slide area. The shelf ranges between 0 and 15 meters depth and it is cut by

several thalwegs with a SW orientation. A second shelf is observed on the south-eastern part of the airport platform. The shelf is prolonged by a steep slope (18-26°), incised by many submarine thalwegs.

The Var Prodelta (location on **Figure 1**) consists of low gradient delta-toe bottomsets, steep coarse to fine grained delta front sets affected by waves and various gravity-driven processes, and topsets up to 80 m thick formed by a succession of muddy laminates and thin peat interbeds overlaying a basal conglomerate (Dubar and Antony, 1995) (**Figure 3**). The basal conglomerate corresponds to Würm last lowstand deposits.

3. The 1979 Nice catastrophe

The Nice international airport was constructed on a platform enlarged by land filling operations. On 16th of October 1979, a part of the airport extension, meant to be a harbour, collapse into the sea. The harbour collapse was accompanied by a tsunami wave of 2-3 meters height (Gennesseaux et al., 1980). This catastrophic event caused the lost of human lives and important material damages. The nearby Monaco observatory did not register any earthquake that could have triggered the slide (Malinverno et al., 1988).

The submarine slide area was surveyed by EM 1000 mapping (Bourillet et al., 1992) and the slide initial volume was estimated to be about 8.7×10^6 m^3 by Assier-Rzadkiewicz et al. (2000), based on the difference between the two bathymetric maps, before and after the 1979 slide. The maximum thickness of sediment is located under the corner of the new harbour construction. The average failure surface observed under the harbour construction ranges between 30 and 40 m water depths (Sultan et al., 2004).

The initial slide quickly transformed into a debris flow and turbidity current by progressive downslope erosion and water incorporation (Mulder et al., 1997). The path of the 1979 event is strongly marked on the upper continental slope by an incised thalweg. This

1 thalweg is 25-40 m depth, 150-300 m wide and 4.5 km long (Mulder et al., 1997) and joins

2 the Var Canyon at 1000 m water depth (**Figure 4**). The flow continued its path through the

3 Var Canyon and the Middle Var Valley and cut two submarine cables 3 h 45 min and 8 h after

4 the initial failure; the cables being located at around 83-87 km and respectively 114 km from

5 the slide area (Hugot, 2000).

6 A sandy fresh sediment deposit, possibly linked to the 1979 event, was mapped by

7 Piper and Savoye (1993) from high resolution seismic profiles. The volume of the sand

8 deposit was estimated to be about $15 \times 10^7 \, \text{m}^3$. Mulder et al. (1997), estimated the total volume

9 of sediment deposited by the 1979 turbidity current at $15 \times 10^8 \, \text{m}^3$, by considering that sand

10 represents only a part of the total deposited volume.

11 To explain the triggering mechanism of the 1979 accident, two different scenarios

12 were proposed. The first scenario, recommended by the MIP (MIP, 1981) suggested that the

13 initial failure occurred on the slope and retrogressively reached the continental shelf. The

14 initial deep failure generated the collapse of the new harbour creating the tsunami wave. On

15 the other hand, the DDE (DDE, 1981) and Seed (Seed, 1983) proposed a different scenario: a

16 tsunami wave was initially generated by a massive slide, around 10^8m^3 (Seed, 1983) located

17 at around 15 km from the coastline. The tsunami wave induced a lowering of the sea level at

18 the coastline level of about 2.5 m (Seed, 1983). The sudden emersion of the harbour created

19 an overload on the slope (submerged unit weight substituted by the total unit weight),

20 sufficient to initiate static liquefaction into loose sand layer present on the continental slope

21 and to generate the harbour collapse.

22 Two numerical models for tsunami and landslide have been developed (Assier-

23 Rzadkiewicz et al., 2000) in order to test the validity of the two proposed scenarios.

24 Retrogressive slide scenario (refer to M.I.P., Habib 1994) showed that the inundation

25 observed in front of the Nice airport could be created by an initial slide of about 10.10^6m^3.

1 However, the wave energy would not have been sufficient to inundate the coast-line off

2 Antibes, according to witnesses' observations. The deep landslide scenario was tested for a

3 landslide with a volume of $70.10^6\,\mathrm{m}^3$, located at the bottom of a canyon 3 km southwest off

4 Nice airport area. Such a landslide occurring approximately at the same time as the slump of

5 the building area, create amplitude and periods of the waves that match with the observation

6 but the chronology of the events is not correctly reproduced. The results of a larger and deeper

7 landslide simulation, better match with some of the whiteness's observations. The case where

8 the initial sediment mass is growing by erosion and assimilation of new material wasn't took

9 into account by Assier-Rzadkiewicz et al. (2000).

10 Slope stability assessment of the Nice area was carried out using bathymetric data

11 acquired before the 1979 event (Sultan et al., 2001). Under static conditions the area

12 concerned by the 1979 event remains stable (Factor of Safety > 1). For a sea-level lowering of

13 2.5 m, the Factor of Safety decreases with respect to gravitational loading but remains greater

14 than 1.

15 Several surveys were conducted after the 1979 event. The Escyanice 06 dive was

16 realized at 18 km from the 1979 slide on the eastern flank of the Upper Valley (location on

17 **Figure 1**) where an ancient bathymetric map (SHOM, France) indicated a lowering of the

18 seafloor with respect to new detailed bathymetric data (Pautot, 1981). Furthermore, it was the

19 only area able to explain the Seed and DDE hypothesis. No evidences of fresh massive slide

20 or erosive features were observed. However, the Seed's scenario remains the "official" truth.

21 It is curious that the two proposed hypotheses of the 1979 event did not consider the

22 role played by the harbour embankment loading in terms of strain generation and mechanical

23 behaviour of the sediment from the continental shelf.

24

25 **4. Materials and Methods**

1   4.1. Materials

2   The data used for this study (**Figure 4)** are obtained essentially from different

3   IFREMER campaigns and are complemented by industrial CPTU data (Sols Essais, 1994).

4   The first swath bathymetric survey took place in November 1979, on the R/V Jean

5   Charcot (Pautot, 1981). The present swath bathymetric data represents a compilation of

6   different type of data: SeaBeam (1979), EM 1000 (1991) andd EM 300 (2000). The before

7   1979 DEM (Digital Elevation Model) is a compilation of pre-failure mono-beam bathymetric

8   data for depth ranging between 0 and 150 m and post-failure data for the deeper part

9   (Bourillet, 1991).

10   Submersible dives were conducted six months after the 1979 event, during Escyanice

11   cruise (Escyanice, 1980), completed later by other submersible surveys (Same, 1986 and

12   Monicya, 1989) (**Figure 4**).

13   Deep-towed side-scan sonar imagery and 3.5 kHz profiles have been also collected

14   during the SAME cruise in 1986 (Same, 1986) with the French S.A.R. (Système Acoustique

15   Remorqué). The S.A.R. side-scan antenna has a mean 200 kHz frequency and the vehicle is

16   towed at about 100 m above the seafloor. The survey covers a surface of 1300 km^2, but for

17   this study, we will only use the lines collected on the upper slope (**Figure 4**).

18   Four sediment cores located on the upper slope have been recovered during two recent

19   oceanographic surveys (GMO and Geosciences II) (Sultan et al., 2004) (**Figure 4**). More

20   recently, in September 2005, the 1979 slide scarp has been sampled. Two Kullenberg cores

21   (KENV2-01, KENV2-02) (**Figure 4**) were acquired in order to characterize the physical and

22   geotechnical properties of the sediment from the failure plane. Sediment core KENV2-01 was

23   collected just under the corner of the new harbour construction and the other one, KENV2-02,

24   250 meters westwards.

1   In addition, CPTU in-situ measurements, made at the airport platform (**Figure 4**),

2   completed the data set (Sols Essais, 1994).

3   <u>4.2. Methods</u>

4   The physical and mechanical properties of the sediment were determined with

5   different tools and tests, such as, the Multi Sensor Core Logging (http://www.geotek.co.uk)

6   (density or unit weight, compressional wave velocities, and magnetic susceptibility), the laser

7   grain-size analyser, vane shear test, water content measurements, Atterberg limits,

8   consolidation tests, etc.

9   The geomechanical properties of the sediment allow to create a lithological model of

10   the airport platform and basement. The geometry of this lithological model along dip was

11   constrained with previous works (L'Homer, 1980; Dubar and Antony, 1995) and results from

12   the present work. The slope geometry and lithology determination was an essential element

13   for the assessment of the Nice slope stability and the evaluation of the Factor Of Safety

14   (*FOS*).

15   The FEMUSLOPE software (Sultan et al. 2001) was used to assess the slope stability.

16   This software is based on the finite elements method. The soil is considered as a Mohr-

17   Coulomb elastic, perfectly plastic material. The yield function *f* is defined by the following

18   expression:

19

20   $$f = p\sin\phi + q\left(\frac{\cos\theta}{\sqrt{3}} - \frac{\sin\theta\sin\phi}{3}\right) - c'\cos\phi \qquad [\,1\,]$$

21

22   where *c'* is the drained cohesion, *φ'* is the internal friction angle, *p*, *q* and *θ* are respectively

23   the first, second and third stress invariants. The calculation is carried out under the hypothesis

24   of plane deformation.

25   In the limit equilibrium method the *FOS* is described as:

1

$$FOS = \frac{\text{resisting force (or moment)}}{\text{driving force (or moment)}} \qquad [\,2\,]$$

3   Using the finite element method, the determination of the *FOS* consists in calculating

4   the maximum displacement for various values of *FOS*. The *FOS* is used to reduce the shear

5   strength parameters *c'* or *Su* (cohesion or undrained shear strength) and *φ'* (internal friction

6   angle) according to the following equations to bring the slope to a limiting state or failure:

$$c_{FOS} = \frac{c'}{FOS} \qquad [\,3\,]$$

$$\varphi_{FOS} = \tan^{-1}\left(\frac{\phi}{FOS}\right) \qquad [\,4\,]$$

9   c_{FOS} and φ_{FOS} are the partial shear strength parameters.

10   The value of *FOS* corresponding to a sudden increase in displacement is considered as

11   the critical *FOS*. Failure is considered to occur theoretically for a *FOS* equal or less than 1. In

12   natural environment, a *FOS* less than 1 is impossible, since the slope failure occurs at *FOS*

13   equal to 1. With the proposed method, the traditional definition of the *FOS* is conserved so

14   that the results can be directly compared with other methods. In addition to the *FOS*, the Finite

15   Element Method (FEM) allows the determinations of the stress tensor, the displacement field

16   and the yield function. Zero or positive yield function *f* characterizes sediments undergoing

17   plastic deformation.

18

19   **5. Results**

20   5.1. Morphology

21   Four main thalwegs characterize the area between the Var Canyon and the Median

22   Valley and they are shown in **Figure 5** (1 to 4 from west to east). The different thalwegs are

23   incised in their upper part and become larger (from 50-90 m to 200-300 m) close to their

confluences with the Var Canyon. The third thalweg is directly connected to the 1979 slide scar. Dotted line from **Figure 5** represents the possible path of the 1979 flow down the continental slope.

We present on **Figure 5** an interpretation from the submersible dives: Escyanice 08 and 13 (Escyanice, 1980), Same 60 (Same, 1986) and Monicya 75 (Monicya, 1989) and from the side-scan sonar images (Same, 1986). Fresh erosion marks on the sea-floor were observed after the 1979 Nice failure based on the submersible data. Anthropogenic material and marl blocks were observed in a bend, located middle slope (black stars on **Figure 5**) (Monicya, 1989). These materials are certainly coming from the airport embankment. During the Monicya cruise, dive n° 75 (see location on **Figure 4**), important accumulations of marl blocs coming from the walls of the third thalweg were observed (pink circles on **Figure 5**). They are testifying the destabilization of the walls by turbiditic flow, possibly the 1979 flow.

At the confluence with the Var Canyon, accumulations of significant rock blocks are observed (Escyanice, 1980; Same, 1986). Limestone or conglomerate blocks are not coming from a known outcrop in the area. They correspond to blocks which were used to protect the airport embankment. We supposed that the energy of the 1979 flow was powerful enough to transport blocks of more than 1 meter diameter down to the Var Canyon.

The Var Canyon floor is covered by boulders, gravels and sand deposits (**Figure 5**) (Same, 1986). Lineaments pointed out at the base of the slope (**Figure 5**) represent the crests of gravel waves which were observed on the SAR images (Same, 1986) and during the submersible dives (Escyanice, 1980).

Evidences of massive accumulations, such as debris-flows deposits, were not observed on the thalwegs floors. It seems that, the thalwegs were by-pass zones for the 1979 event and that the 1979 flow increases its volume by erosion of the thalwegs floors and walls, continuing its path through the Var Canyon.

1   The large number of small tributaries and thalwegs entrenching the Var upper slope

2   show that the 1979 event is not a so singular event in the area. The area seems to be affected

3   by important erosion processes and events like the 1979 event might have been frequent in the

4   past.

5

6   5.2. Sediment analyses

7   5.2.1. Sedimentary description

8   Sediment samples located on the upper part of the continental slope have been

9   described by Sultan et al. (2004) (MD01-2470, MD01-2471, KGMO-03 and KGMO-06)

10   (**Figure 4**). The cores description put in evidence the presence of detrital silty carbonates with

11   some silty to fine sand quartz, few calcareous nannoplancton and occasional plant debris and

12   gastropods (turittela) in the upper part (Sultan et al, 2004). These sedimentary facies are

13   similar to those described by Dubar and Antony (1995). Corrected AMS radiocarbon dating a

14   wood fragment at 3.52 mbsf, gave sedimentation rates of 11.5 m.ky^{-1} for the area located near

15   the 1979 slide (Sultan et al., 2004). The sedimentation rates are very high but in the same

16   range as those calculated from Dubar and Anthony (1995).

17   The two cores collected during the ENVAR2 cruise (KENV2-01, KENV2-02) are the

18   first sediment samples collected on the 1979 slide scar (**Figure 4**). Sediment cores were

19   collected to establish the lithology and mechanical behaviour of the sediment from the failure

20   surface of the 1979 event.

21   **Figure 6** (a, b) shows a comparison of the seafloor before the 1979 event and present-

22   day seafloor. We estimate a maximum thickness of removed sediments, based on the two

23   bathymetric maps (before and after 1979) of about 38 m for the core KENV2-01, and about

24   28 m for the other one, KENV2-02.

1   Sediment core KENV2-01 is 2.28 m long (**Figure 7**). The upper part, from 0 to 1.75

2 m, is characterized by thin to medium sand content with values ranging between 15 and 90%.

3 A layer characterized by coarse sand and 1-3 cm diameter pebbles has been observed between

4 0.90 and 0.97 mbsf. Below 1.75 m depth, the deposits are silty clay dominated (**Figure 7-c**).

5 Parallel- coloured (grey to red) clay laminaes characterize the lower part of the core (**Figure**

6 **7-b**). The core KENV2-01 is characterized by high unit weight with values of 19 kN/m^3 at

7 surface, and between 20 and 22 kN/m^3 for the rest of the core (**Figure 7-d**), while the

8 compression wave velocity Vp increases slightly with depth. The Vp values measured on the

9 MSCL range between 1500-1560 m/s on the upper part and 1600-1650 m/s in its lower part

10 (**Figure 7-e**). The coarse sand layer observed between 0.90 and 0.97 mbsf is characterized by

11 a peak of about 26 kN/m^3 and a compression wave velocity of 2400 m/s (measured on the

12 MSCL).

13   The sediment core KENV2-02 is 1.38 m long (**Figure 8-a**). The grain-size distribution

14 plot (**Figure 8-c**) shows an important sand content (20-90 %). Sand deposits have been

15 described in the upper part of the core KENV2-02. The first sequence between 0.10 and 0.15

16 m depth is characterized by 5 cm thick coarse, yellow, non graded sand deposit. This

17 sequence overlies almost 20 cm of massif coarse sand and pebbles. The pebbles can reach 6

18 cm in diameter. The sequence presents a sharp and erosive basal contact. Three non graded

19 sand deposits alternate with coloured thin parallel clay laminaes (between 0.35 and 0.80

20 mbsf) (**Figure 8-b**). The lower part of the core is characterized by mottled facies resulting

21 from the mixture of silty clay and discontinuous sand laminaes. The same facies was

22 described by Sultan et al. (2004) on cores collected on the upper continental slope (MD01-

23 2470, MD01-2471, KGMO-03 and KGMO-06, see figure **Figure 4** for location).

24   The upper 10 cm of sediment in core KENV2-02 are characterized by a unit weight,

25 from 17 kN/m^3 to 20 kN/m^3, followed by higher unit weight values in the coarse sand and

1　pebbles layer. Below 0.35 mbsf the unit weight range between 20 and 22 kN/m^3 (**Figure 8-d**).

2　The *Vp* measurements shows values between 1500-1700 m/s, only the sand and pebbles layer

3　is reaching a maximum *Vp* of 2400 m/s (from the MSCL) (**Figure 8-e**).

4

5　5.2.2. Geotechnical parameters

6　　　**Figure 9** presents a comparison between the geotechnical properties of the cores

7　collected on the upper slope (MD01-2470 and MD01-2471) and the two cores collected from

8　the slide scar (KENV2-01 and KENV2-02). **Figure 9** shows the undrained shear strength (*Su*)

9　measured only on clay and silty clay sediment, the sensitivity defined as the ratio between

10　maximum undrained shear strength (*Su*) and the remoulded undrained shear strength (*Su*$_{rem}$)

11　and the *Su/σ'*$_v$ ratio where *σ'*$_v$ is the vertical effective stress. The *Su* of the ENVAR 2 cores is

12　higher than the Geosciences II cores (**Figure 9-a**). For the sediment core KENV2-01, the

13　undrained shear strength (*Su*) increases linearly with depth from 5 kPa at the seafloor level to

14　10 kPa at 0.9 mbsf (**Figure 9-a**). Below the sand layer (beneath 0.97 mbsf), the *Su* shows a

15　linear increase with depth, with a maximum *Su* of around 34 kPa at 2.20 mbsf. For the

16　sediment core KENV2-02, *Su* of 5 kPa was measured above the sand deposits (0.10 mbsf).

17　Below the sand deposits, the measurements of the undrained shear strength show values of *Su*

18　between 9 kPa at 0.82 mbsf and more than 21 kPa at 1.1 mbsf.

19　　　**Figure 9-b** presents the sensitivity values calculated for the four sediment cores. The

20　high sensitivity of the sediment from the scar stands out. Sensitivity values, from the sediment

21　cores KENV2-01 and KENV2-02, are 2 to 3 times higher than the sensitivity values measured

22　on cores MD01-2470 and MD01-2471.

23　　　**Figure 9-c** presents the *Su/σ'*$_v$ ratio calculated for the four sediment cores. It seems

24　that the values on the sediment core MD01-2470 and MD01-2471 are inferior to 1; only the

25　upper sediment is characterized by values superior to 1. The *Su/σ'*$_v$ ratio calculated for the

1 two ENVAR 2 cores is higher than 1 and shows the over-consolidated nature of the sediment

2 (**Figure 9-c**).

3

4 5.2.3. Consolidation geotechnical tests

5   Samples from cores KENV2-01 and KENV2-02 were taken at different depths in

6 order to perform 4 oedometer tests (KENV2-01 at 0.14, 0.60 and 1.37 mbsf; KENV2-02 at

7 0.91 mbsf) (see white rectangles on **Figure 7** and **Figure 8**).

8   **Figure 10** presents the oedometer tests performed on sediment samples from KENV2-

9 01 and KENV2-02. Under 25 kPa of vertical effective stress, the circulation of fresh water

10 within the sediment induced an important vertical collapse of the following three samples:

11 KENV2-01 at 0.6 and 1.37 mbsf and KENV2-02 at 0.91 mbsf (**Figure 10**). The oedometer

12 test performed on the sample acquired at 0.14 mbsf from core KENV2-01 was not affected by

13 the fresh water circulation due to the moderate sensitivity of the sediment. The collapse of the

14 three other samples is related to the high sensitivity of the sediment as it can be seen from

15 **Figure 9-b**. Indeed, in saturated sensitive clays, collapsive structure and sediment

16 deformation may be generated by electro-chemical changes induced by pore-water leaching

17 (Lefebvre, 1995).

18   **Table 1** presents the results from the four consolidation tests showing the Over

19 Consolidation Ratio (*OCR*) calculated from the effective vertical stress and the

20 preconsolidation effective stress ($OCR = \sigma'_p/\sigma'_v$). The *OCR* ranges from 55.6 at the top of the

21 sedimentary column to 11.21 at 1.37 mbsf on the core KENV2-01 and it is about 21 at 0.91

22 mbsf on the core KENV2-02. The *OCR* values highlight the over-consolidated nature of the

23 sediment.

24

25 5.3. In-situ piezocone test

1   In 1994, Sols Essais carried out along the Nice coast four in-situ piezocone tests (Sols

2   Essais, 1994). One of the secondary applications of the piezocone measurement is the

3   determination of the stratigraphy and the lithology of buried sediment. Pore pressure is

4   difficult to interpret in terms of lithology. A soft clay, as well as a contractive silt, react to the

5   penetration of the rod by generating a high pore pressure. On the other hand, very stiff clay, as

6   well as very dense silty clay or a dilative silt respond in the same way in term of pore pressure

7   i.e. a low or even a negative pore pressure. However, thanks to the combination of the 3

8   classical CPT sensors measurements (tip resistance, sleeve friction and pore pressure), it is

9   possible to define a sediment classification chart (see for instance Campanella et al., 1982;

10   Robertson et al., 1986; Robertson, 1990 and Ramsey, 2002 among others). In order to define

11   the sediment type from the CPTU pz11 data, we have used in this work the diagram proposed

12   by Ramsey (2002).

13   In **Figure 11,** the corrected cone tip resistance (q_t), the differential pore water pressure

14   (Δu), and the sleeve friction (fs) profiles for the PZ11 test are presented (for location refer to

15   **Figure 4**). The tip resistance profile shows peaks (**Figure 11-a**) associated with a decrease of

16   pore pressure (**Figure 11-b**), and indicating the presence of coarse-grained sediment. On the

17   other hand, low values of the sleeve friction are observed below 30 mbsf (**Figure 11-c**).

18   **Figure 11-d** shows different facies associated to the PZ 11 cone penetration profile. It is

19   interesting to point out the existence of a sensitive clay below 30 mbsf. The sensitive clay

20   layer depth, from 30 to 45 mbsf, coincides to the average depth of the failure surface. On the

21   same diagram (**Figure 11-d**) we can point out the presence of a very thin sand layer located at

22   around 36-37 mbsf into the sensitive clay layer. This predicted lithology matches well with the

23   lithology of cores collected in the 1979 scar.

24

25   5.4. Geological-geotechnical model

1   Geotechnical data from PZ11 site are selected to create a vertical lithological profile

2   essential for the numerical modelling. The lithological profile is divided into 14 layers and

3   each layer is characterized by different mechanical properties (see **Table 2**).

4   When sediment is sheared under an applied stress, excess pore pressure is generated

5   that may (drained conditions) or may not (undrained conditions) dissipate depending on the

6   permeability of the sediment and the time available. The 1979 slope failure occurred after a

7   short period of the harbour construction. That is why in this work we have decided to evaluate

8   the slope stability of the Nice slope by considering the undrained mechanical parameters of the

9   clay layers (undrained shear strength) and the drained parameters for cohesionless soils

10   (internal friction angle).

11   The lithology and thickness were estimated from PZ 11 lithological model (**Figure 11-**

12   **d**). Estimation of the undrained shear strength (Su) for clayey layers was made based on the

13   CPTU data according to the following equation:

14   $$Su = \frac{q_{net}}{Nk}$$ [5]

15   where q_{net} is the net cone resistance that depends on the tip resistance qc, the in-situ vertical

16   effective stress, and the effective cone section ratio. Nk (assumed to be 12 in this case) is an

17   empirical cone factor that depends on lithology (e.g., Lunne et al., 1997). Clay and silty clay

18   layers are characterized by Su corresponding to the average value measured for each layer

19   during the PZ 11 CTPU test.

20   Shear strength of cohesionless soils, sand and silt, is usually expressed in terms of the

21   internal friction angle (φ'). Numerous methods for assessing φ' from cone resistance have been

22   published (Lunne et al., 1997). We used the empirical method proposed by Campanella and

23   Robertson (1983) to determine φ' from the cone resistance (q_c) and the vertical effective stress

24   (σ'_v). Layer 12 is the last sedimentary layer characterized by geotechnical parameters

25   identified thanks to the CPTU measurements. In the lack of any geotechnical data below layer

12, two case calculations were considered: 1) layers 13 and 14 as the substratum and were

artificially characterized by high undrained shear strength and 2) only layer 14 was considered

as a substratum while the lithology of layer 13 was assumed similar to layer 11.

6. Modelling the Nice airport slope failures

6.1. Input data

In order to evaluate the slope stability before the 1979 accident, two cross-sections

along *ENE–WSW* and *NW–SE* directions, have been selected based on the bathymetric

analysis (for location see **Figure 6**). Comparison between the present-day seafloor surface

and that before the 1979 accident on the Nice airport area, reveals a significant thickness of

missing sediment (**Figure 6- c** and **Figure 6-d**).

For the two cross-sections, the problem domain is discretized into 4517 nodes and

1428 quadrilateral elements. Mesh and limit conditions are presented in **Figure 12**.

Three scenarios were considered in order to identify the triggering mechanism responsible of

the 1979 failure:

1- The first scenario considers the stability of the slope before the harbour extension.

2- The second scenario considers the load induced by the embankment of the new

harbour. The unit-weight of the first layer changed, due to the embankment loading.

The aim of this modelling is to quantify the impact of the new harbour construction on

the sediment. We also modelled the Seed hypothesis, by considering the loading of the

new harbour induced by 2.5 m sea level lowering.

3- The third scenario simulates the softening/creeping of the sediment with the maximum

strains generated by the harbour extension. Based on the results from the embankment

1   loading case, we imposed the softening of the sensitive clay layer by decreasing the

2   undrained shear strength.

3

4   6.2. Output data

5   Different parameters are resulting from the numerical models and the main ones being:

6   a. The *FOS* which is defined from the diagram *FOS* vs. maximum displacement on curve

7   presented in **Figure 13**. The critical *FOS* corresponds to a sudden increase in displacement.

8   b. The yield function with positive values corresponding to the plastic behaviour of the

9   sediment is also presented for the critical *FOS*.

10   c. The horizontal displacements are presented for the critical *FOS*.

11

12   6.3. Results

13   6.3.1. Scenario 1: Slope stability assessment before the harbour extension

14   To identify the origin of the 1979 slope failures and to get a reference calculation, the

15   *FOS* is calculated by considering only the submerged sediment unit weight (γ) along the two

16   considered directions (gravity loading). For this scenario, layers 13 and 14 were considered as

17   rigid substratum.

18

19   (a) The ENE – WSW cross section

20   For the ENE-WSW direction, the critical *FOS* is equal to 1.8 (**Figure 13 a**). **Figure**

21   **14-1a** presents the yield surface values and shows the existence of a continuous area of plastic

22   deformation (yellow areas). Therefore, failure might occur for partial shear strength

23   parameters corresponding to a *FOS* of 1.8. Curiously, and despite the stable state of the

24   considered slope (ENE-WSW), the most critical failure surface matches well with the present

25   location of the seafloor (orange line in **Figure 14-1a**).

1   **Figure 14-1c** shows the results of the horizontal displacement calculated for a *FOS*

2   equal to 1.8. The maximum displacement is located along the slope and it is about 0.05 m

3   (**Figure 14-1c**).

4   (b) The NW – SE cross section

5   For the NW-SE cross-section, the *FOS* corresponding to a sudden increase of the

6   maximum displacement is equal to 1.45 (**Figure 13-b**). **Figure 15-1a** shows a continuous area

7   of plastic deformation, where yield surface values are positive.

8   **Figure 15-1b** presents the horizontal displacement determined for a *FOS* equal to

9   1.45. The displacement values are higher than for the ENE – WSW direction; with a maximum

10   horizontal displacement located in the upper part of the slope and it is about 10 cm.

11   The *FOS* reveals to be higher than 1 before the harbour extension (1.8 and 1.45

12   respectively) along the two directions. The analysis however reveals the metastable state of

13   the upper Nice slope (*FOS* = 1.45). For this reason, the origin of the sediment failures in the

14   study area is more difficult to assess if we consider the probably large volume of sediments in

15   a metastable state. Any external load may generate sediment failures. The same conclusion

16   was obtained by Mulder (1992).

17

18   6.3.2. Scenario 2: Slope stability assessment after the harbour extension

19   The second scenario aims to evaluate the slope stability under the embankment

20   loading where the harbour geometry and its additional load are considered in the calculation.

21   The geotechnical parameters of the 14 soil layers used in this calculation test are the same as

22   for the previous case. Only the total unit weight value of the first layer corresponding to the

23   harbour embankment (total unit weight, $\gamma = 26$ kN/m^3) has been added.

1   <u>(a) The ENE – WSW direction</u>

2   For the first calculation, layers 13 and 14 were considered corresponding to the

3 substratum. **Figure 13-a** shows the variation of the maximum displacement vs the *FOS* along

4 the ENE-WSW profile. The sudden increase of the maximum displacement occurs for a *FOS*

5 equal to 1.8 (**Figure 13-a**). The embankment did not generate any increase of the *FOS*

6 (around 1.8 before and after the harbour extension) only the maximum displacement

7 increased.

8   **Figure 14-2a** is presenting the yield function calculated for a *FOS* of 1.8. The plastic

9 behaviour characterized by positive values (yellow areas) describes a continuous area from

10 the shelf to the slope (**Figure 14-2a**). The base of the critical surface seems to be rooted in

11 layer 12, which corresponds to the sensitive clay (**Figure 14-2a**).

12   Comparison between **Figure 14-1a** (1st scenario) and **Figure 14-2a** (2nd scenario)

13 confirms the increase of the volume of metastable sediment, with an expansion of the critical

14 failure surface from the slope to the shelf.

15   **Figure 14-2b** presents the horizontal displacement calculated for the present scenario

16 (*FOS* = 1.8). We observed that the horizontal displacement expanded beneath the harbour

17 embankment. The maximum value of the horizontal displacement is 0.055 m. Comparison

18 between the seafloor after the 1979 accident and the most critical failure surface obtained

19 from the calculation confirms again that the slope failure occurred in 1979 coincides with the

20 predicted most critical failure surface (**Figure 14-2b**).

21   An additional calculation where only layer 14 was considered as rigid has shown that

22 the slope is characterized by a *FOS* between 1.7 and 1.8 and the base of the critical surface is

23 once again initiated in layer 12.

24

1   (b) The NW – SE direction

2   **Figure 13-b** shows the variation of the maximum displacement vs *FOS* under the

3   embankment loading conditions. The *FOS* values is now equal to 1.3 and shows a decrease

4   comparing to the previous case (**Figure 13-a**). For this calculation, layers 13 and 14 were

5   considered corresponding to the substratum.

6   **Figure 15-2a** show the yield function calculated for a *FOS* of 1.3. We observe that

7   sediment masses characterized by plastic deformation are now activated beneath the harbour

8   embankment and prolonged into the very sensitive clay layer. **Figure 15-2b** presents the

9   horizontal displacement and shows high horizontal displacements beneath the harbour

10   embankment (**Figure 15-2b**). The maximum value of the horizontal displacement is about 11

11   cm.

12   The position of the substratum with respect to the sensitive layer seems to have a

13   minor effect on the *FOS* and the position of the critical failure surface. That is why for the

14   following scenarios only the first layer geometry where the substratum corresponds to layer

15   13 and layer 14 will be considered.

16   (c) NW-SE direction under Seed's hypothesis

17   According to Seed's hypothesis (Seed, 1983; Habib, 1994), a slide, with a significant

18   initial volume, initiated 15 km off the coastline, induced the lowering of the sea level of about

19   2.5 m, which in turn increased the load of the harbour embankment. In this section, the Seed's

20   hypothesis is considered using the additional load resulting from a sea level lowering of 2.5

21   m. Under this hypothesis, the loading mechanism consists of replacing, over the first 2.5 m,

22   the submerged unit weight (γ') of the sediment (and or embankment) by the total unit weight

23   (γ).

1   **Figure 13-b** shows that the *FOS,* calculated for the Seed's hypothesis, is equal to 1.25.

2   It seems that the *FOS* remains almost unchanged comparing with the previous case (**Figure**

3   **13-b**).

4   **Figure 16-a** presents the yield function and shows the area where the sediment is

5   characterized by a plastic behaviour. Continuous area rooting in layer 12 is observed beneath

6   the embankment and on the slope (**Figure 16-a**). Comparison between **Figure 16-a** (Seed's

7   hypothesis) and **Figure 15-2a** (embankment load) shows the activation of sediment mass with

8   plastic behaviour on the slope edge under the sea level lowering.

9   **Figure 16-b** presents the horizontal displacement calculated for a *FOS* equal to 1.25.

10   Comparison between **Figure 16-b** and **Figure 15-2b** shows little increase of the horizontal

11   displacement beneath the harbour embankment. The maximum value is now about 13 cm

12   comparing to the 11 cm for the previous case calculation (**Figure 15-b**).

13   Due to the short period under which sea level lowering occurred (Habib, 1994), the

14   small increase in horizontal displacement for a quasi constant *FOS* cannot play an important

15   role in the 1979 slope failure.

16   Simulation results indicate that the harbour extension (embankment load) on the slope

17   had the following effects on the stability of the slope:

18   o   A decrease of the *FOS*, from 1.45 to 1.3, for the *NW – SE* cross section;

19   o   An extension of the plastic area (positive yield function) beneath the harbour

20   embankment

21   o   An increase of the horizontal displacement beneath the harbour extension.

22   The metastable state of the upper Nice slope before the harbour construction is accentuated

23   after the new harbour construction. The Seed's hypothesis (Seed, 1983) did not imply a

24   significant degradation of the upper Nice slope stability. However, Seed supposed that the

25   overloading of the airport platform has generated a static liquefaction of a loose sand layer.

From our in situ geotechnical measurements and coring, no such a loose sand layer was identified. That is why, for our modelling we only considered the embankment emersion as a consequence of the sea level lowering.

6.3.3. Scenario 3: Slope stability assessment under a static load and the creep of the sensitive clay layer

The low FOS characterizing the $NW-SE$ cross-section and the existence of a sensitive clay have probably favoured sediment failure. Although, the FOS is greater than 1 for the two considered cross-sections, creep may induce failures in clayey slopes even for strengths lower than the peak strength (Lefebvre, 1981; Tavenas et al., 1978).

Indeed, soil creep represents strain increases with time resulting from prolonged application of a constant stress. The soil strength along a critical surface when subjected to continuous strains will degrade and the residual strength can reach the remoulded strength of the materials. Geometric changes and associated degradation of strength may then lead to slope failure if the stress state is located above a threshold given by the large deformation strength of the material (Vaunat and Leroueil, 2002).

Creep is generally divided into three stages (see **Figure 17-a**, after Singh and Mitchell, 1968):

- the primary creep starts at a rapid rate and slows with time. Mitchell (1964), among others, adapted the rate process theory to describe this first creep stage.

- the secondary creep has a relatively uniform rate;

- the tertiary creep has an accelerated creep rate and terminates when the material breaks or ruptures. Lefebvre (1981) proposed the concept of a "stability threshold", defined as the strength at about 8% axial strain. Lefebvre (1981) hypothesised that at

1	constant deviatoric stress levels above the threshold value, failure would eventually

2	occur due to creeping.

3	Several empirical models have been proposed for creep-induced failure in materials (see

4	for instance Singh and Mitchell, 1968 and Tavenas et al., 1978). Hunter and Khalili (2000)

5	have proposed a simple criterion, which is presented in **Figure 17-b** and it corresponds to:

6	-	Creep to failure can occur at less than peak strength, with the limiting strength

7		possibly being as low as the fully softened (or critical state) strength.

8	-	The level of shear strain at which the onset of failure due to creep occurs is equivalent

9		to the shear strain at peak stress (ε_{peak}) in the equivalent conventional strength test.

10	**Figure 18-a** presents the deviatoric stresses (q) before and after the harbour extension,

11	along the observed failure surface of 1979 (corresponding to the present seafloor) for a *FOS*

12	equal to 1. From **Figure 18-a**, one can observe a significant increase in deviatoric stress (q)

13	beneath and due to the harbour embankment.

14	**Figure 18-b** shows the variation of the deviatoric stress (q), vs. the shear strain (ε_d) along

15	the 1979 failure surface. In addition to the increase of the deviatoric stress (q), there is also an

16	increase in shear strain (ε_d). For a given ε_{peak} to failure, as defined by the criterion of Hunter

17	and Khalili (2000), **Figure 18-b** shows that the harbour extension decreased the creeping

18	strain needed to initiate failure of the upper Nice slope.

19

20	The NW-SE direction

21	As it was expected from the *FOS* value obtained for the *NW-SE* cross-section and

22	under embankment load conditions, a decrease of the undrained shear strength of about 15 %

23	($1-\dfrac{1}{FOS}$) was needed to generate failure (**Figure 19-a**). This decrease of the undrained shear

24	strength can be generated by the creeping of the sensitive clay layer under the embankment

25

load. Sediment mass characterized by plastic deformation (positive yield function) is activated under the harbour embankment and prolonged into the sensitive clay layer (**Figure 19-b**).

Figure 19-c presents the horizontal displacement calculated for a *FOS* equal to 1. The horizontal displacement is located along the slope and beneath the embankment, and the maximum value is about 9 cm (for *FOS* = 1).

Table 3 summarized the main results obtained from the numerical modelling. One can point out the evolution of the *FOS* values and the horizontal displacement calculated for each study case. The calculation results will be discussed in the next section.

7. Discussion

The present study substantially improves our understanding of the triggering mechanism of the 1979 failure event. Mulder et al. (1997) considered that the Var deep-sea fan is very active and fed by 3 different types of processes: (1) hyperpycnal plumes which are directly linked to the activity of the rivers, (2) high-frequency superficial failures affecting under-consolidated sediments on upper slopes and (3) low-frequency failures affecting larger volumes of sediment generated by external forcing.

7.1. Preconditioning factors

Several factors, related to the geological context, may influence the stability of the Var Prodelta slope:

- Sediment lateral variability

Presently, the head of the submarine canyon is directly connected to the Var River mouth. We know that ephemeral river mouth bars exists and that during huge river floods they collapse into the sea feeding the Var canyon (Sage, 1976). Most of the coarse grained material

is thus trapped into the canyon head. However, under westerly waves conditions, a substantial part of the Var River plume is dispersed over the shelf in front of the airport providing fine sand, silt and mud in that area (Sage, 1976).

Before 1969 when the Var River mouth was fixed with artificial levees, it used to migrate along the coast line over distances of a few kilometres. This migration would have increased through time the heterogeneity of the superficial sediment cover. The lateral variability of sand layers is undocumented,, although it would locally have a great impact on sediment instability. Indeed, these sandy layers could represent the fresh water conduits generating the increase of the sensitivity of the surrounding clay layers and therefore the formation of weak layers in the area.

- Steep slopes and major erosion of the slope

The continental slope in front of the Var prodelta is steep and that considerably increases the risk of slope failure. The Var prodelta slope is undercut by numerous thalwegs. Four main thalwegs characterize the area between the Var canyon and the airport platform. These thalwegs are sharply incised in their upper part and quite large (150-200 meters) close to the confluence with the Var Canyon. The thalwegs are characterized by numerous tributaries, very narrow, some of them being initiated at middle-slope. Other thalwegs are observed eastward the continental slope off the Nice airport.

This clearly indicates that submarine failures are common features along the front of the Var delta and that this phenomenon started long before the airport construction. The undercutting creates local steep slopes that may later trigger the flank collapses.

- Hyperpycnal flows

1   Marine hyperpycnal flows were defined for the first time by Bates in 1953.

2   Hyperpycnal flows may form at a river mouth when the density of the fresh water with

3   substantial suspended mater is superior to the density of the ambient sea water (Bates, 1953;

4   Wright, 1977; Nemec, 1995; Mulder et al., 2003).

5   Mulder et al. (1997) demonstrated that hyperpycnal flows are frequent on the Var area.

6   The Var River is a relatively small river draining the south Alps. Its drainage basin contains

7   extended black shales areas that provide easily erodable particles that can be transported in

8   suspension down to the river mouth. Flash floods are frequent in spring and autumn generally

9   linked to violent storms over the Alps. Statistical analysis of the Var River discharge over the

10   last 40 years showed that the Var River can produce 24 h long hyperpycnal flows into the

11   canyon head every 20 years (Mulder et al., 1997). For example, the volume of sediment

12   delivered at the river mouth during the 1994 flood was about 10 times the average volume of

13   sediment delivered each year. Presently, in-situ monitoring is made along the Var Canyon in

14   order to measure the energy, the frequency and the sediment supply of the currents (ENVAR-

15   Hermes Programme). The impact of such flows on the sediment stability has not been studied

16   yet.

17

18   **7.2. Triggering mechanisms**

19   • Increase of the pore pressure

20   Two weeks before the 1979 event, intense rainfall occurred over the whole Var

21   drainage basin and the Nice coast. This might have increase substantially the pore pressure

22   into the sand layers below the platform and thus decreased the effective stress. However the

23   link between the rainfall water infiltration and the pore pressure in sandy layers below the

24   airport is not well documented but it can be inferred from the location of fresh water springs

25   in Present Day's Nice slope. In-situ piezometer measuremens were conducted by Guglielmi

1   (1993) on the continental slope off the Nice airport in order to quantify the location of fresh

2   water spring. Guglielmi (1993) showed that below the Nice airport the alluvial water flows

3   into the permeable sand layers intercalated within the deltaic Holocene clay deposits.

4

5   •   Anthropogenic actions, such as the airport construction on the shelf or dams and

6   embankment on the Var River

7   Land filling operations on the shelf off Nice started for the first time in 1940, in order

8   to extend the Nice airport on the left bank of the Var River. These works implied the

9   deviation of the Var River mouth westward. Airport expansion gained 50 km^2 to sea in 1969.

10   After 1969, the airport extended off the left bank (Sage, 1976). According to the same study,

11   the airport extension and the urbanization has completely changed the near shore water

12   circulation. Sage (1976) pointed out the influence, that the airport construction would have on

13   the coastal current pattern and on the sediment distribution in the Baie des Anges. The

14   embankment of the Var River, particularly at the river mouth, fixed the link between the river

15   and the canyon head.

16   After construction of the airport, sediment delivered by the river arrived directly at the

17   canyon head. However, in the mean time, several dams were built along the Var River valley

18   in order to trap coarse sediments (pebbles and boulders). The impact of these dams on the

19   sediment content and volumes delivered at the river mouth has not been accurately

20   documented. However, we may assume that volumes of coarse material and coarseness of

21   sediment delivery decreased dramatically because of the dams.

22   Numerical simulations were conducted in this study in order to point out the impact of

23   the harbour construction on the slope stability. The first calculation carried out with the finite

24   elements model, highlighted the metastable state of the Nice slope even before the harbour

25   construction. The *FOS* was found greater than 1, but not enough to presume that the slope was

safe. However, by considering the load induced by the construction of the harbour embankment, the safety conditions become more critical. Moreover, the sediment mass characterized by the plastic deformation (positive yield function) was activated beneath the harbour embankment and an important increase of the horizontal displacement is observed just below the harbour embankment. The critical surface seems to initiate in layer 12, corresponding to the sensitive clay layer.

Although, the embankment generated a tiny decrease of the critical *FOS*, an important increase of the deviatoric stress (q) beneath the airport, due to the harbour embankment was pointed out. In addition to this increase of the deviatoric stress (q), we can clearly see an increase of the shear strain ε_d. Thus, for a given ε_{peak} driven to failure as defined by the criterion of Hunter and Khalili (2000), we see that the harbour extension decreased the creeping strain needed to cause failure of the upper Nice slope. Without the airport embankment, the Nice slope would have probably failed (due to the sensitive clay layer), but probably at a much later stage (without knowing the creeping rate we cannot define more precisely any time period).

- <u>Analysis of the sensitive clay layer</u>

The geotechnical measurements (in-situ CPTU tests and laboratory consolidation tests) pointed out the presence of a sensitive clay layer. A sensitive clay is the result of slow geological processes. Most quick (sensitive) clays have been formed in sediments that were deposited in sea water during the last deglaciation. The clay deposits can be leached, thereby changing ion concentration in the pore water. Leaching can be caused by fresh water infiltration, artesian water pressure in underlying permeable layers and by diffusion.

A sand layer was described in cores KENV2-01 and KENV2-02 within the upper sediments close to the sensitive clay layer. This sand layer represents a very permeable level,

1 which might be a fresh water conduit into the sediment layers. It is therefore probable, that the

2 sensitive clay changed its mechanical properties by leaching due to the fresh water

3 circulation.

4   The 3 oedometer tests carried out on samples from KENV2-01 at 0.60 and 1.37 mbsf

5 and KENV2-02 at 0.91 mbsf showed the same behaviour of sediment collapse and

6 deformation under pure water circulation. This hydro-mechanical behaviour confirms the

7 presence of a high sensitive clay at the failure interface of the 1979 event.

8   In our model results, the critical surface seems to be initiated in layer 12, which

9 corresponds to the sensitive clay layer. Seafloor surface after the 1979 accident coincides with

10 the most critical failure surface obtained from the calculation.

11

12 **7.3. Most probable scenario of slope failure**

13   In view of the circumstances that concurred before the Nice 1979 catastrophic event, the

14 most probable scenario was (**Figure 20**):

15   1. The occurrence of a high permeability sand layer in the 1979 scar wall is a major

16   preconditioning factor. This layer probably acted as a fresh water conduit, as it was

17   observed by Guglielmi (1993), which caused an increase of the clay sensitivity (by

18   leaching) and a decrease of the effective stress (**Figure 20-a**).

19   2. Taking into account the load induced by the harbour construction, the embankment

20   probably generated softening of the mechanical properties of the sensitive clay layer

21   and an increase in creeping (**Figure 20-b**).

22   3. Possible increase of the pore pressure after a period of rainfall could also play an

23   important role. Pore pressures would induce a decrease of the effective stress and

24   conduct to failure (**Figure 20-c**).

1 Those three factors were enough to trigger the initial slide that secondly evolved into a

2 turbiditic current which probably cut a sharp thalweg into the Var upper slope, incorporating a

3 large volume of new material along its path down the Var Canyon.

4

7.4. Prediction of potential future slope failures

6   For what we know now, there is no doubt, the airport platform area is clearly

7 metastable and several triggering mechanisms are still active. To go ahead and better predict

8 what could happen in the future under different loading conditions, we obviously need to have

9 a better knowledge of the sensitive clay spatial and vertical pattern and of the distribution of

10 sandy layers all over the slope, and particularly below the airport. We believe that the

11 occurrence of this sensitive clay is a highly important observation. Does this layer cover the

12 whole area under the airport platform? Does it become sensitive only within the pathways

13 linked to the proximity of narrow sandy channels? We cannot answer these questions using

14 today available data; however, these are certainly crucial questions for assessing the present

15 stability state of the airport platform.

16   We also need to get a better knowledge of the spatial and temporal pore pressure

17 variations in some sandy layers that might be fed by the Var River discharge and rainfall

18 water. A monitoring of microtopography evolutions offshore the airport platform might also

19 help tracking the precursory signs of slope instability.

20   Since the 1979 event was not triggered by an earthquake, we did not take into account

21 earthquakes as possible triggering mechanism. However, this area may be affected by

22 moderate earthquakes (Magnitude up to 7). Under cyclic loading, the sediments dynamic

23 behaviour is controlled by the sediment characteristics (grain-size distribution, presence or

24 absence of a clay fraction, etc…), and by the intensity and duration of the cyclic loading

25 (Sultan et al., 2004). For sand and silty sands, a cyclic shaking may induce a phenomenon of

liquefaction. The depositional pattern of sand and silt in the first hundred meters of sedimentary column is not documented at an accurate scale today.

Acquisition of high resolution (sparker) and very high resolution (chirp mud penetrator) seismic lines across the Var delta platform and upper slope would also be necessary to be able to make assumptions regarding the stability of the upper slope under earthquake loading.

8. Conclusion

In 1979, a catastrophic event occurred on the Nice continental slope (French Riviera) generating the lost of human lives and important material damages. Part of the new harbour that was in construction at the edge of the International Airport of Nice has collapsed into the sea. The aim of this paper is to describe the 1979 event and to re-evaluate the slope stability of the near Nice harbour area.

The main results of this study are:

1. New sediment cores coming from the 1979 slide scar were used to determine the mechanical properties of the sediments left behind the 1979 slide. We put in evidence the presence of a layer (KENV2-01 and KENV2-02, see figure 7) having a sensitivity 2 to 3 times higher than the surrounding sediment (MD01-2470 and MD01-2471, see figure 7).

2. The first calculation using the finite element model, highlights the metastable state of the Nice slope even before the harbour construction took place. The *FOS* is greater than 1, but not enough to presume that the slope is safe.

3. After embankment loading, a sediment mass characterized by plastic deformation (positive yield function) is activated under the harbour embankment and prolonged into the very sensitive clay layer (layer 12). Furthermore, an important increase of the

1   horizontal displacement takes place under the harbour embankment. The critical

2   surface seems to initiate in layer 12, which corresponds to the sensitive clay layer. The

3   seafloor after the 1979 accident coincides with the most critical failure surface

4   predicted from the numerical calculations.

5   4. Failure of the Nice slope may take place for a decrease of only 15% of the undrained

6   shear strength (Su) due to softening of the sensitive clay layer.

7   5. Our modelling results, showing a relatively long-term failure (by creep), are in good

8   agreement with the official report mentioning that during the landfill operations, 110

9   reports of cracks, settlements, failures and embankment collapse occurred.

10   6. The 1979 Nice harbour accident was probably initiated by the combination of several

11   factors: the load of the harbour embankment, the circulation of fresh water in the

12   permeable sand layer and the creeping of the sensitive clay layer.

13

23

24

1 **References**

2

3 Assier-Rzadkiewicz, S., Heinrich, P., Sabatier, P.C., Savoye, B., Bourillet, J.F., 2000.

4   Numerical modelling of a landslide-generated tsunami: the 1979 Nice event. Pure

5   Applied Geophysics 157, 1707-1727.

6

7 Baptista, M. A., Miranda, P.M.A., Miranda, J.M., Mendes Victor, L., 1998. Constrains on the

8   source of the 1755 Lisbon tsunami inferred from numerical modelling of historical data.

9   J. Geodyn. 25, 159-174.

10

11 Bates, C. C., 1953. Rational theory of delta formation. American Association of Petroleum

12   Geologists Bulletin 37, 2119-2162.

13

14 Bourillet, J. F., 1991. Géomorphologie à partir d'un modèle numérique de terrain (Baie des

15   Anges, Nice). 3rd Cong. Fr. Sedimentology; Brest.

16

17 Bourillet, J. F., Edy, C., Normand, A., 1992. Nouvel ensemble pour la reconnaissance du

18   plateau continental: Sondeur multifaisceaux EM1000 et logiciel Trimus. Un exemple: la

19   Baie des Anges (France). CIESM Rapp. int. Mer Médit.33, 112.

20

21 Bryn, P., Solheim, A., Berg, K., Lien, R., Forsberg, K.F., Haflidason, C.F., Ottesen, D., Rise,

22   L., 2003. The Storegga Slide Complex: repeated large scale sliding in response to

23   clymatic cyclicity. In: Locat, J., Mienert, J. (Eds.), Submarine Mass Movements and

24   Their Consequences. Kluwer Acad. Publ., Dordrecth, The Neterlands, pp. 215-222.

25

1 Campanella, R. G., Gillespie, D., Robertson, P.K., 1982. Pore pressures during cone

2   penetration testing. Proceedings of the 2nd European Symposium on Penetration Testing,

3   ESOPT-2, Amsterdam 2, pp: 507-512.

4

5 Campanella, R. G., Robertson, P.K., 1983. Interpretation of cone penetration tests: Part II:

6   Clays. Can. Geotech. Journ. 20, 734-745.

7

8 Canals, M., Lastras, G., Urgeles, R., Casamor, J.L., Mienert, J., Cattaneo, A., De Battist, M.,

9   Haflidason, H., Imbo, Y., Laberg, J.S., Locat, J., Long, D., Longva, O., Masson, DG.,

10   Sultan, N., Trincardi, F., Bryn, P., 2004. Slope failure dynamics and impacts from

11   seafloor and shallow sub-seafloor geophysical data: case studies from the COSTA

12   project. Marine Geology 213, 9-72.

13

14 Clauzon, G., 1978. The Messinian Var Canyon (Provence, southern France)-paleogepgraphic

15   implications. Marine Geology 27, 231-246.

16

17 Clauzon, G., Suc, J.P., Aguilar, J.P., Ambert, P., cappetta, H., Cravatte, J., Michaux, J.,

18   Roiron, P., Rubino, J.L., Savoye, B., Vernet, J.L., 1990. Pliocene Geodynamic and

19   Climatic Evolutions in the French Mediterranean Region. Paleontologia di Evolucio

20   Memoria Espacial 2, 132-186.

21

22 Cochonat, P., Bourillet, J.F., Savoye, B., Dodd, L., 1993. Geotechnical characteristics and

23   instability of submarine slope sediments, the Nice slope (N-W Mediterranean Sea).

24   Marine Georessources and Geotechnology 11, 131-151.

25

1   DDE, 1981. Rapport de la Direction Departementale de l'Equipement des Alpes-Maritimes

2   du 17 juillet 1981 sur le sinistre du 16 :10 :79. unpublished report.

3

4   Dubar, M., Antony, E.J., 1995. Holocene Environmental Change and River-Mouth

5   Sedimentation in the Baie des Anges, French Riviera. Quaternary Research 43, 329-343.

6

7   Escyanice (1980). Escyanice Cruise Report, IFREMER

8

9   Gennesseaux, M., Mauffret, A., Pautot, G., 1980. Les glissements sous-marins de la pente

10   continentale niçoise et la rupture des câbles en mer Ligure (Méditerranée occidentale).

11   C.R. Acad. Sc. Paris t. 290.

12

13   Guglielmi, Y., 1993. Gydrogéologie des aquifères Plio-Quaternaires de la Basse Vallée du

14   Var. Thèse d'Etat, Académie d'Aix-Marseille, pp. 170.

15

16   Habib, P., 1994. Aspects géotechniques de l'accident du nouveau port de Nice. Revue

17   Française de Géotechnique 65, 3-15.

18

19   Haflidason, H., Sejrup, H.P., Nygard, A., Bryn, P., Lien, R., Berg, K., Masson, D.G., Forberg,

20   C.F., 2004. Architecture, geometry and slide development of the the Storegga Slide.

21   Marine Geology 213, 201-234.

22

23   Hampton, M. A., Lee, H.J., Locat, J., 1996. Submarine landslides. Reviews of Geophysics 34,

24   33-59.

25

1   Heezen, B. C., Ewing, M., 1952. Turbidity currents and submarine slumps, and the 1929

2   Grand Banks earthquake. Am. J. Sci. 250, 849-873.

3

4   Horn, R., Menard, F., Munch, F., 1965. Etude géophysique de la basse vallée du Var. Rapp.

5   DS 65 A37, BRGM Orléans.

6

7   Hugot, A., 2000. Modélisation des écoulements gravitaires catastrophiques par une approche

8   objet dynamique: érosion-transport-dépôt. Thèse, Université Paris 6, pp. 410.

9

10 Hunter, G., Khalili, N., 2000. A simple criterion for creep induced failure of over-

11   consolidated clays. Pro. GeoEng. 2000 Conference.

12

13 Irr, F., 1984. Paléoenvironnements et évolution géodynamique néogènes et quaternaires de la

14   bordure nord du bassin méditérranéen occidental." Thèse d'Etat, Nice, 464 p.

15

16 L'Homer, A., 1980. Etude sédimentologique des carottes des sondages (Nouveau port de

17   Nice). Rapp. ES (10) 03.80, BRGM Orléans.

18

19 Lee, H. J., Schwab, W.C., Edwards, B.D., Kayen, R.E., 1991. Quantitative controls on

20   submarine slope failure morphology. Marine Geotechnology 10, 143-157.

21

22 Lefebvre, G., 1981. Strength and slope stability in Canadian soft clay deposits. Canadian

23   Geotechnical Journal 18, 420-442.

24

25 Lefebvre, G., 1995. Collapse mechanisms and design considerations for some partly saturated

1   and saturated soils. In: E.Derbyshire et al. (Eds.), Genesis and properties of collapsible

2   soils, Kluver Academic Publishers, pp. 361-374.

3

4   Locat, J., 2001. Instabilities along ocean margins: a geomophological and geotechnical

5   perspective. Marine and Petroleum Geology 18, 503-512.

6

7   Locat, J., Lee, H.J., 2002. Submarine landslides: advances and challenges. Can. Geotech.

8   Journ. 39, 193-212.

9

10   Lunne, T., Robertson, P.K., Powell, J.J.M., 1997. Cone Penetration Test in Geotechnical

11   Practice, Blackie Academic and Professional, UK, 312 pp.

12

13   Maliverno, A., Ryan, W.B.F., Auffret, G., Pautot, G., 1988. Sonar images of the path of

14   recent failure events on the continental margin off Nice, France. Geol. Soc. Am. Spec.

15   Pap 229, 59-75.

16

17   Masson, D. G., Canals, M., Alonso, B., Urgeles, R., Huhnerbach, C., 1998. The Canary

18   Debris Flow: source area morphology and failure mechanism. Sedimentology 45, 411-

19   432.

20

21   MIP, 1981. Mission d'Inspection Pluridisciplinaire sur le sinistre de Nice du 16 Octobre 1979,

22   Rapport final. Unpublished report.

23

24   Mitchell, J. K., 1964. Shearing resistance of soils as a rate process. Journal of the Soil

25   Mechanics and Foundations Division, ASCE, 90, 29-61.

1

2   Monicya, 1989. Monicya Cruise Report, IFREMER

3

4   Mulder, T., 1992. Aspects géotechniques de la stabilité des marges continentales. Application

5   à la Baie des Anges, Nice, France. Thèse, Institut National Polytechnique de Lorraine.

6   193 pp.

7

8   Mulder, T., Savoye, B., Syvitski; J.P.M., 1997. Numerical modelling of a mid-sized gravity

9   flow: the 1979 Nice turbidity current (dynamics, processes, sediment budget and seafloor

10   impact). Sedimentology 44, 305-326.

11

12   Mulder, T., Syvitski, J.P.M., Migeon, S., Faugères J.-C., Savoye, B., 2003. Marine

13   hyperpycnal flows: initiation, behaviour and related deposits. A review. Marine and

14   Petroleum Geology 20, 861-882.

15

16   Nemec, W., 1995. The dynamics of deltaic suspension plumes. In: Oti, M.N., G Postma (Eds.)

17   Geology of Deltas, pp. 31-93.

18

19   Pautot, G., 1981. Carte morphologique de la Baie des Anges, Modèle d'instabilité de pente

20   continentale. Oceanologica Acta 4, 203-212.

21

22   Piper, D. J. W., Shor, A.N., Farre, J.A., O'Connell, S., Jacobi, R., 1985. Sediment slides

23   around the epicentre of the 1929 Great Banks earthquake. Geology 13, 538-541.

24

25   Piper, D. J. W., Savoye, B., 1993. Processes of late Quaternary turbidity current flow and

1 deposition on the Var deep-sea fan, north-west Mediterranean Sea. Sedimentology 40,

2 557-582.

3

4 Piper, D. J. W., Cochonat, P., Morrison, M.L., 1999. The sequence of events around the

5 epicentre of the 1929 Great Banks earthquake: initiation of debris flow and turbidity

6 current inferred from sidescan sonar. Sedimentology 46, 79-97.

7

8 Ramsey, N., 2002. A calibrated model for the interpretation of cone penetration tests (CPTs)

9 in North Sea quaternary soils. Proc. Offshore Site Investigation and Geotechnics:

10 diversity and Sustainability, London, UK, pp. 341-356.

11

12 Robertson, P. K., Campanella, R.G., Gillespie D., Grieg, J., 1986. Use of Piezometer cone

13 data, Proceedings, Use of In-situ Tests in Geotechnical Engineering (In-situ '86). GSP,

14 American Society of Civil Engineers, New York 6.

15

16 Robertson, P. K., 1990. Soil classification using the cone penetration test. Can. Geotech.

17 Journ. 27, 151-158.

18

19 Sage, L., 1976. La sédimentation à l'embouchure d'un fleuve côtier méditerranéen. Le Var.

20 Thèse, Université de Nice, 243 pp.

21

22 Same, 1986. Same Cruise Report, IFREMER

23

24 Savoye, B., Cochonat, P., Olliver, G., Auffret, G.A., Bourillet, J.F., 1989. The submarine Var

25 Canyon (French Riviera): Detailed study of the activity of a modern canyon. Regional

1   Meeting of Sedimentlogy, Budapest (1989).

2

3   Savoye, B., Piper, D.J.W., 1991. The Messinian event on the margin of the Mediterranean Sea

4   in the Nice area, southern France. Marine Geology 97, 279-304.

5

6   Savoye, B., Piper, D.J.W., Droz, L., 1993. Plio-Pleistocene evolution of the Var deep-sea fan

7   off the French Riviera. Marine and Petroleum Geology 10, 550-571.

8

9   Seed, B. H., 1983. Recheche de la cause du glissement du Port de Nice, survenu le 16 :10 :79.

10   Unpublished report.

11

12   Singh, A., Mitchell, J.K., 1968. General stress strain time function for soils. J. Soil Mech.

13   Found. Eng. Div. ASCE, SM1, pp 21-43.

14

15   Sols Essais, 1994. Sols Essais Internal Report.

16

17   Sultan, N., Cochonat, P., Bourillet, J.F., Cayocca, F., 2001. Evaluation of the Risk of Marine

18   Slope Instability: A Pseudo-3D Approach for Application to Large Areas. Marine

19   Georessources and Geotechnology 19, 107-133.

20

21   Sultan, N., Cochonat, P., Canals, M., Cattaneo, A., Dennielou, B., Haflidason, H., Laberg,

22   J.S., Long, D., Mienert, J., Trincardi F., Urgeles, R.,, Vorrene, T.O., Wilson, C., 2004.

23   Triggering mechanisms of slope instability processes and sediment failures on continental

24   margins: a geotechnical approach. Marine Geology 213, 291– 321.

25

1   Tavenas, F., Leroueil, S., La Rochelle, P., Roy, M. (1978). Creep behaviour of an undisturbed

2   lightly overconsolidated clay. Canadian Geotechnical Journal 15, 402-423.

3

4   Vaunat, J., Leroueil, S., 2002. Analysis of Post-Failure Slope Movements within the

5   Framework of Hazard and Risk Analysis. Natural Hazards 26, 83–109.

6

7   Wright, L. D., 1977. Sediment transport and deposition at river mouths; a synthesis.

8   Geological Society of America Bulletin, 88, 857-868.

9

1 **Table captions:**

2

3 Table 1: Geotechnical parameters used for the finite element calculation

4 Table 2: Results from the consolidation tests

5 Table 3: Summary of the results obtained from the numerical modelling

6

7 **Figure captions:**

8

9 Figure 1: General bathymetric map of the Ligurian Sea and the Var sedimentary system

10 showing its main features (Mercator, WGS 1984)

11
12 Figure 2: Bathymetric map showing a zoom on the continental shelf and the 1979 slide area

13 (Mercator, WGS 1984).

14

15 Figure 3: Schematic cross section of the Var Holocene delta, from Dubar and Anthony

16 (1995).

17

18 Figure 4: Bathymetric map showing the available data: side scan sonar data (Same, 1986) and

19 submersible dives: Escyanice 08 et 13 (Escyanice, 1980); Same 60 (Same, 1986) and

20 Monicya 75 (Monicya, 1989). (Mercator, WGS 1984)

21

22 Figure 5: Interpretation of the submersible observation and side scan sonar data. Fresh erosion

23 marks and blocks accumulations are observed on the 1979 flow path (red lines)

24 (Mercator, WGS 1984).

25

26 Figure 6: (a) Contour maps before 1979 accident and (b) after the 1979 accident showing the

27 change on the slope morphology and the ENVAR2 cores location: (c) ENE-WSW cross-

28 section showing the seafloor surface before and after the 1979 event and KENV2-02
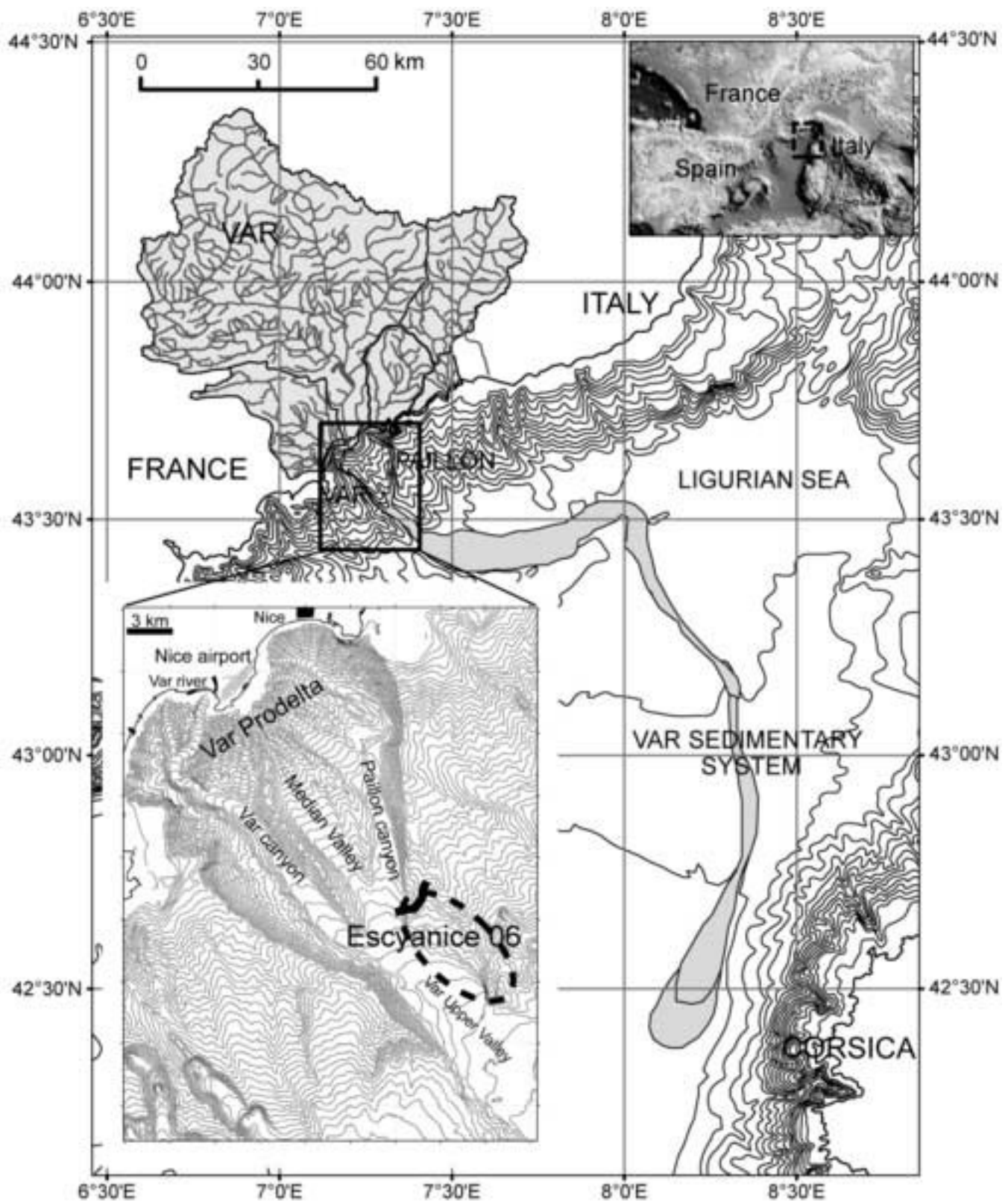
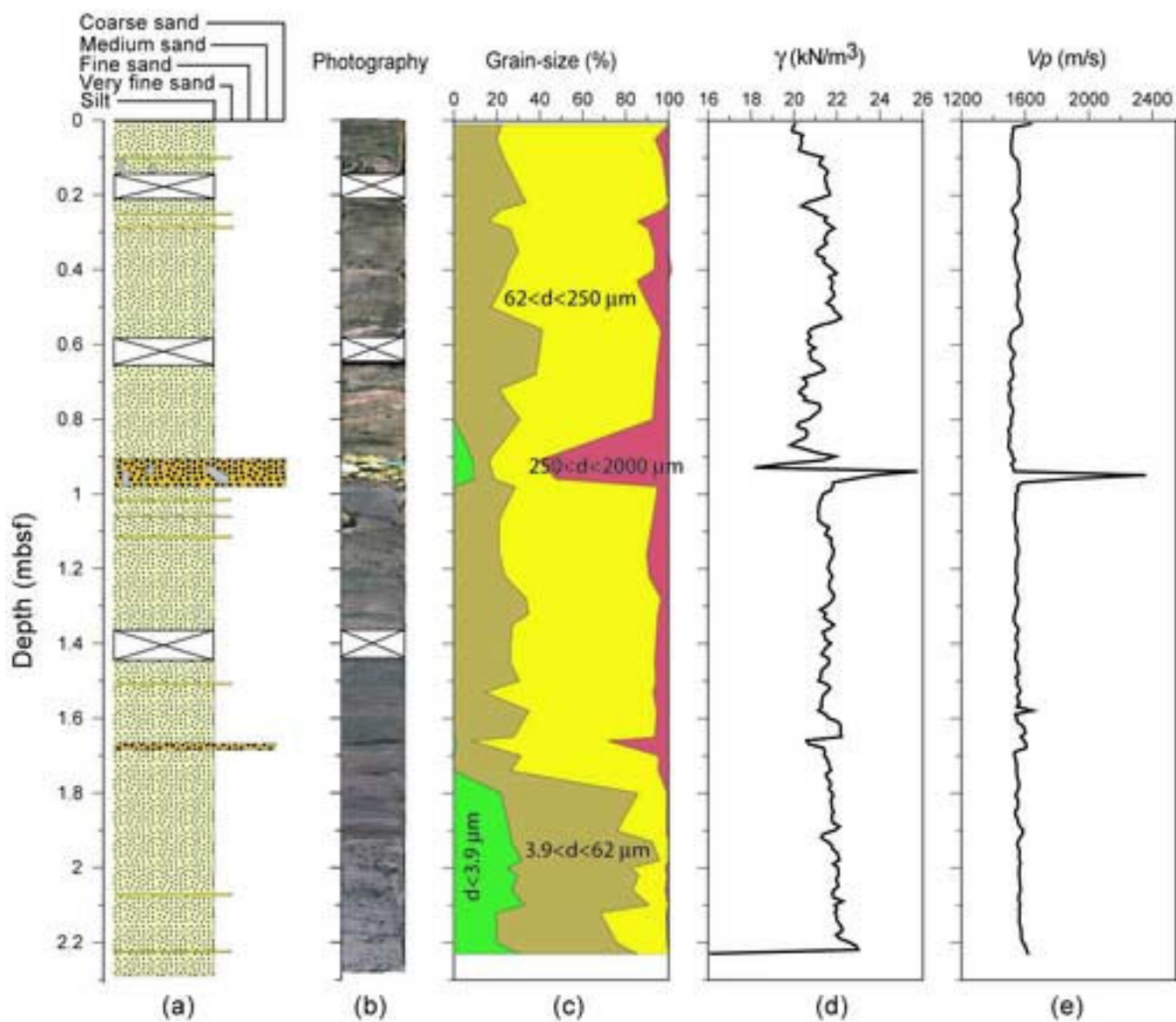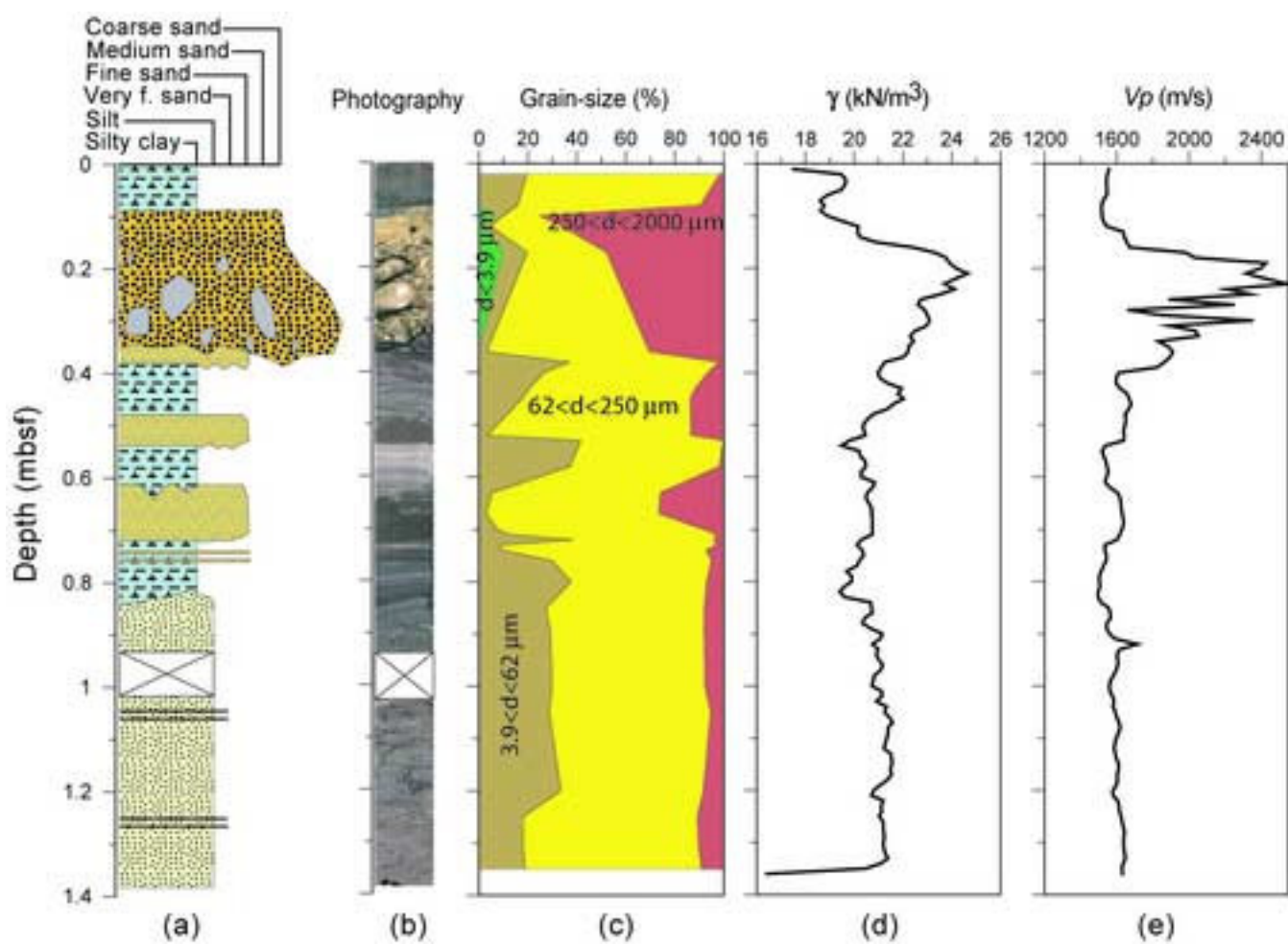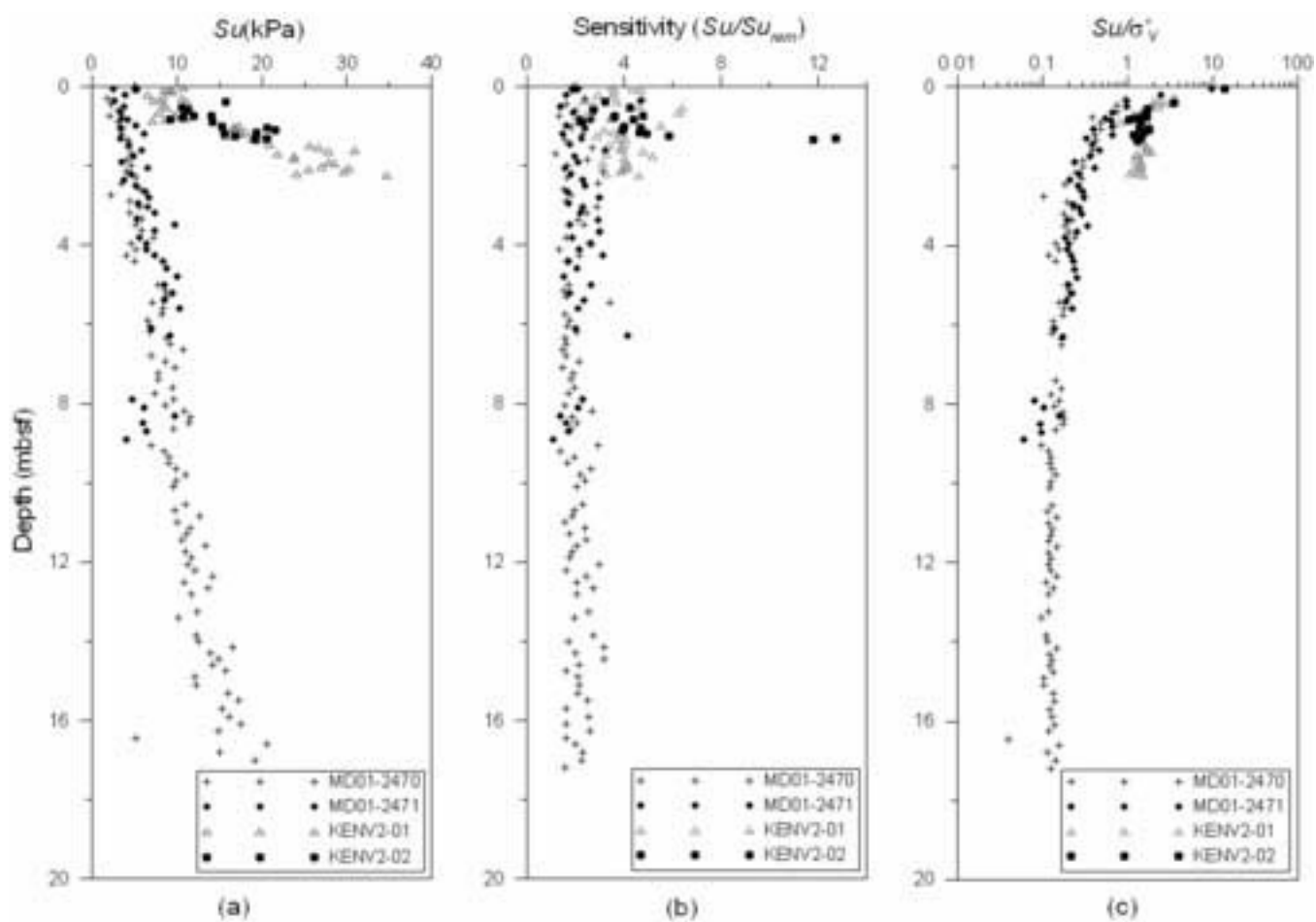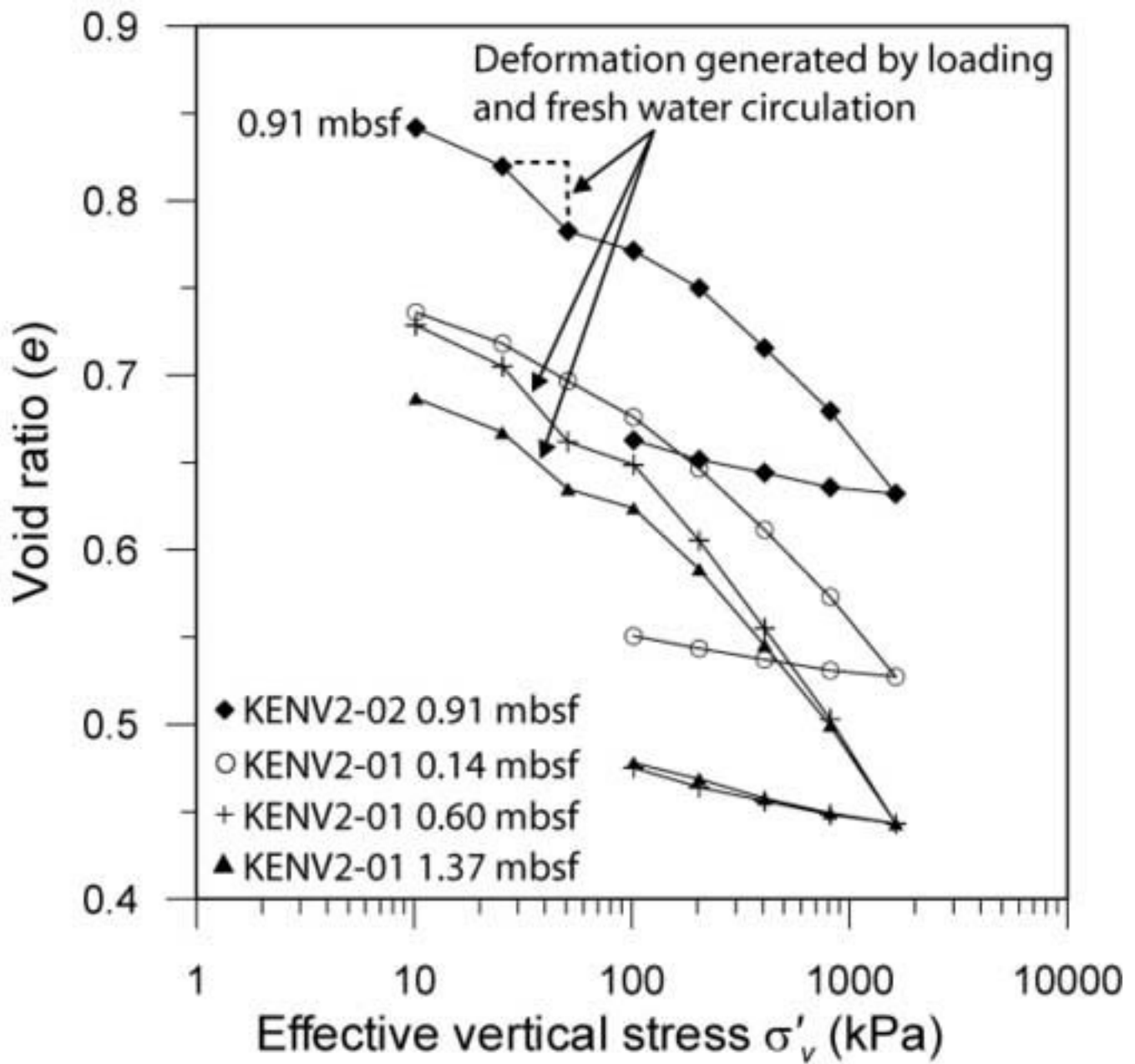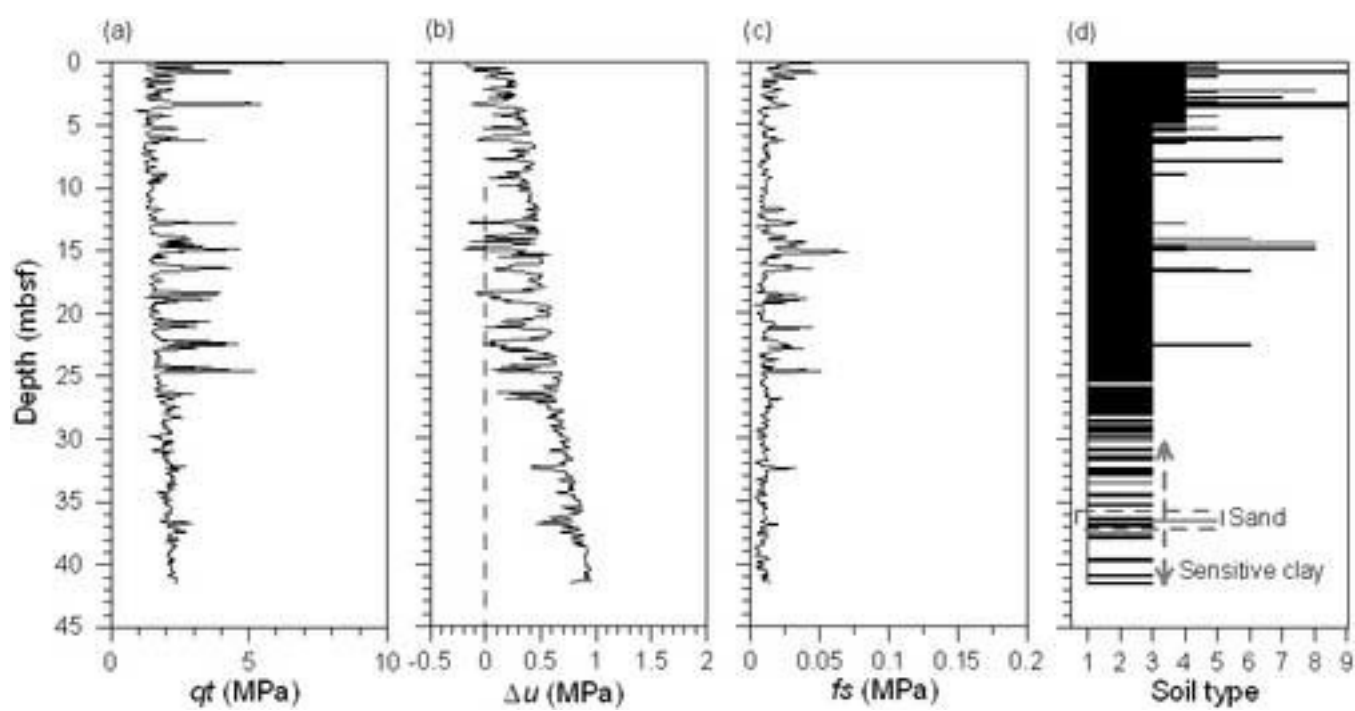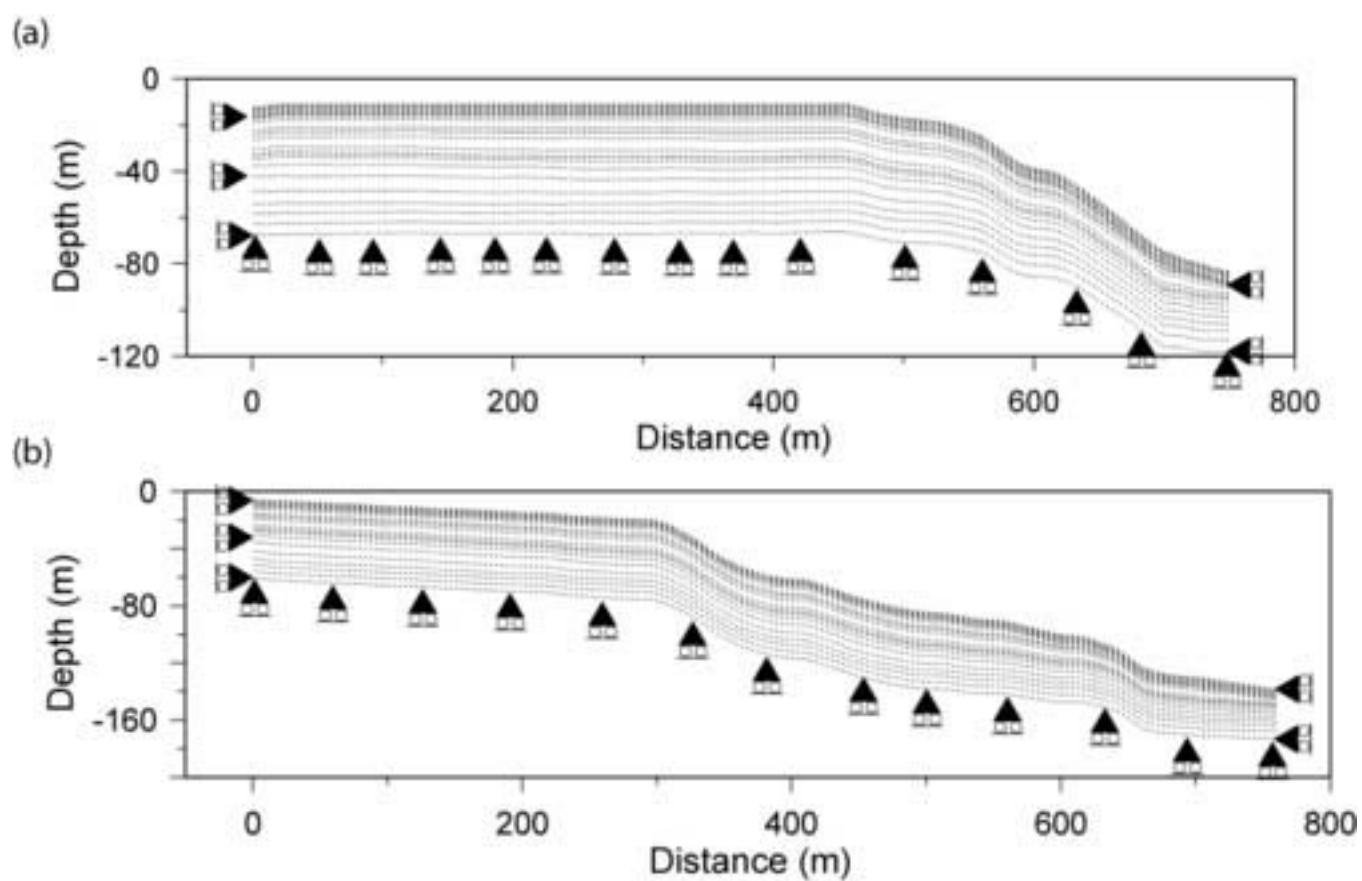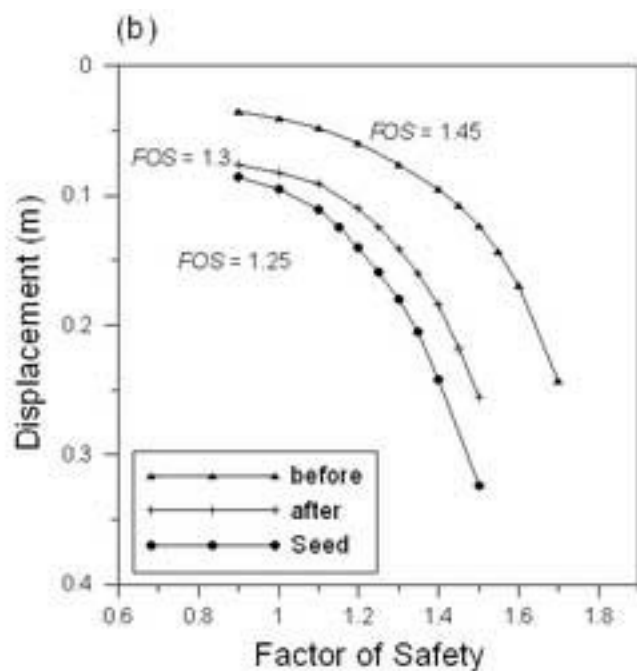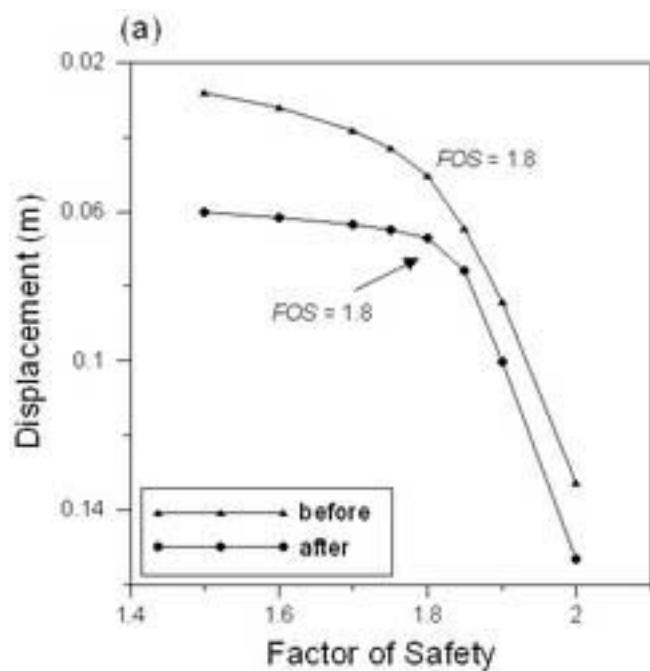**Figure 2**
Click here to download high resolution image
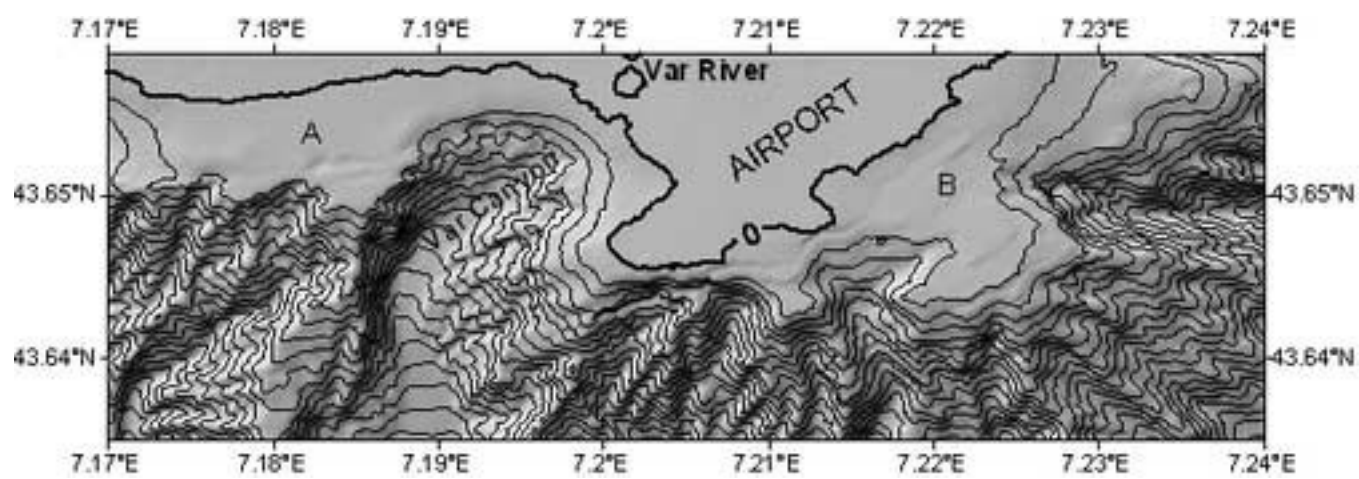
Figure 3
Click here to download high resolution image
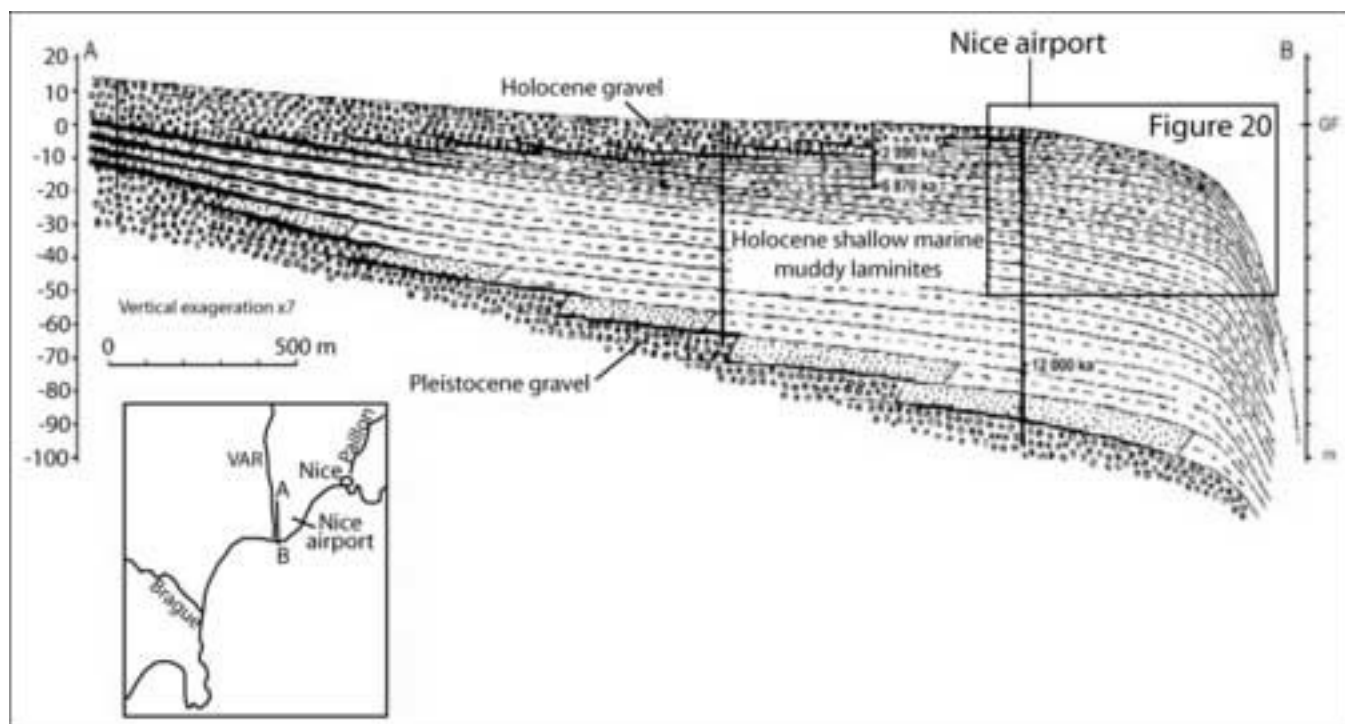
Figure 5

(a)

(b)

(c)
ENE   WSW

Before 1979 event
seafloor

38 m

KENV2-01

Present seafloor

(d)
NW   SE

28 m

Present seafloor

KENV2-02

Before 1979 event seafloor

(a)　(b)　(c)　(d)　(e)

Coarse sand
Medium sand
Fine sand
Very f. sand
Silt
Silty clay

Photography   Grain-size (%) γ (kN/m^3)   Vp (m/s)

Depth (mbsf)

(a)   (b)   (c)   (d)   (e)
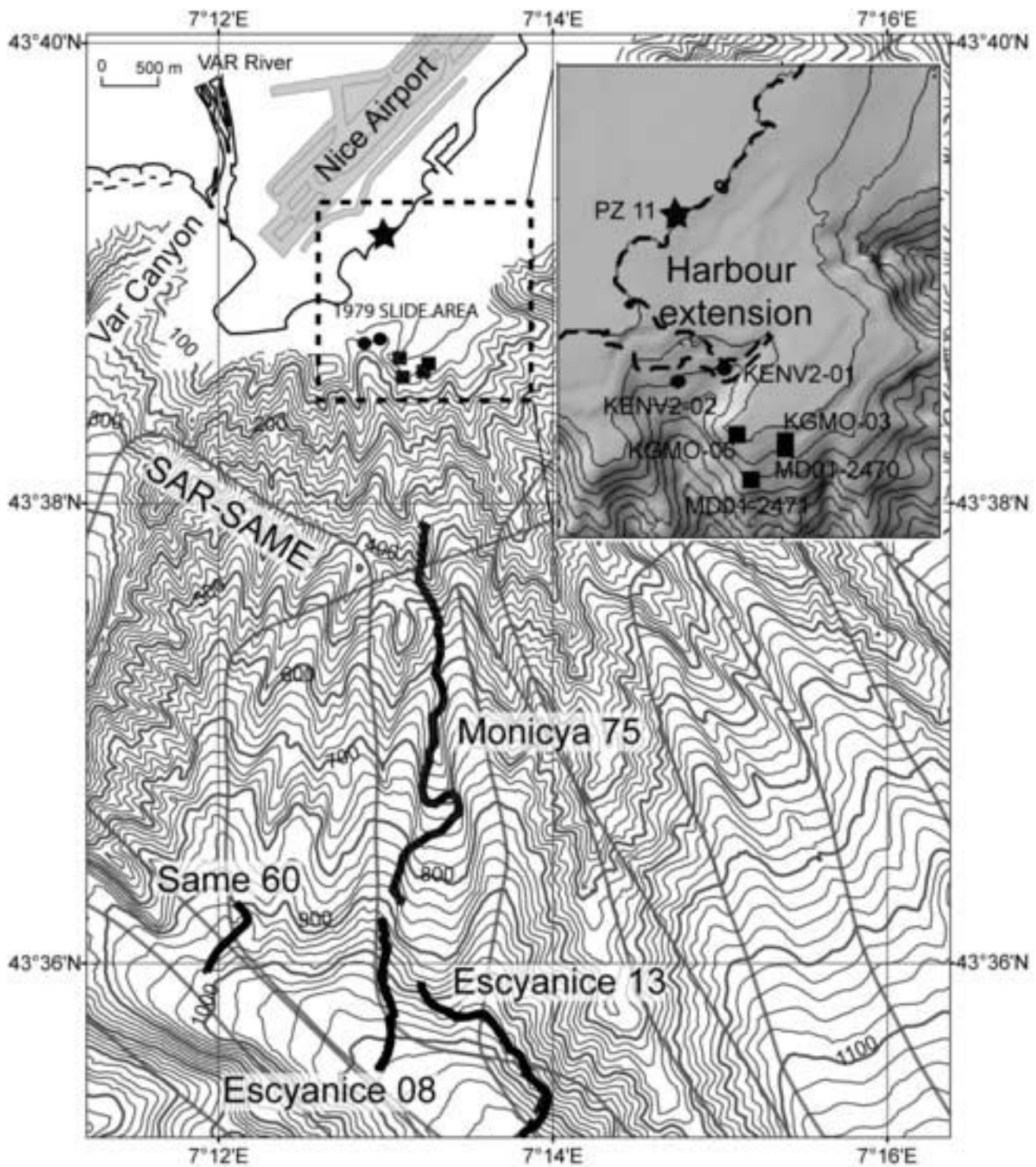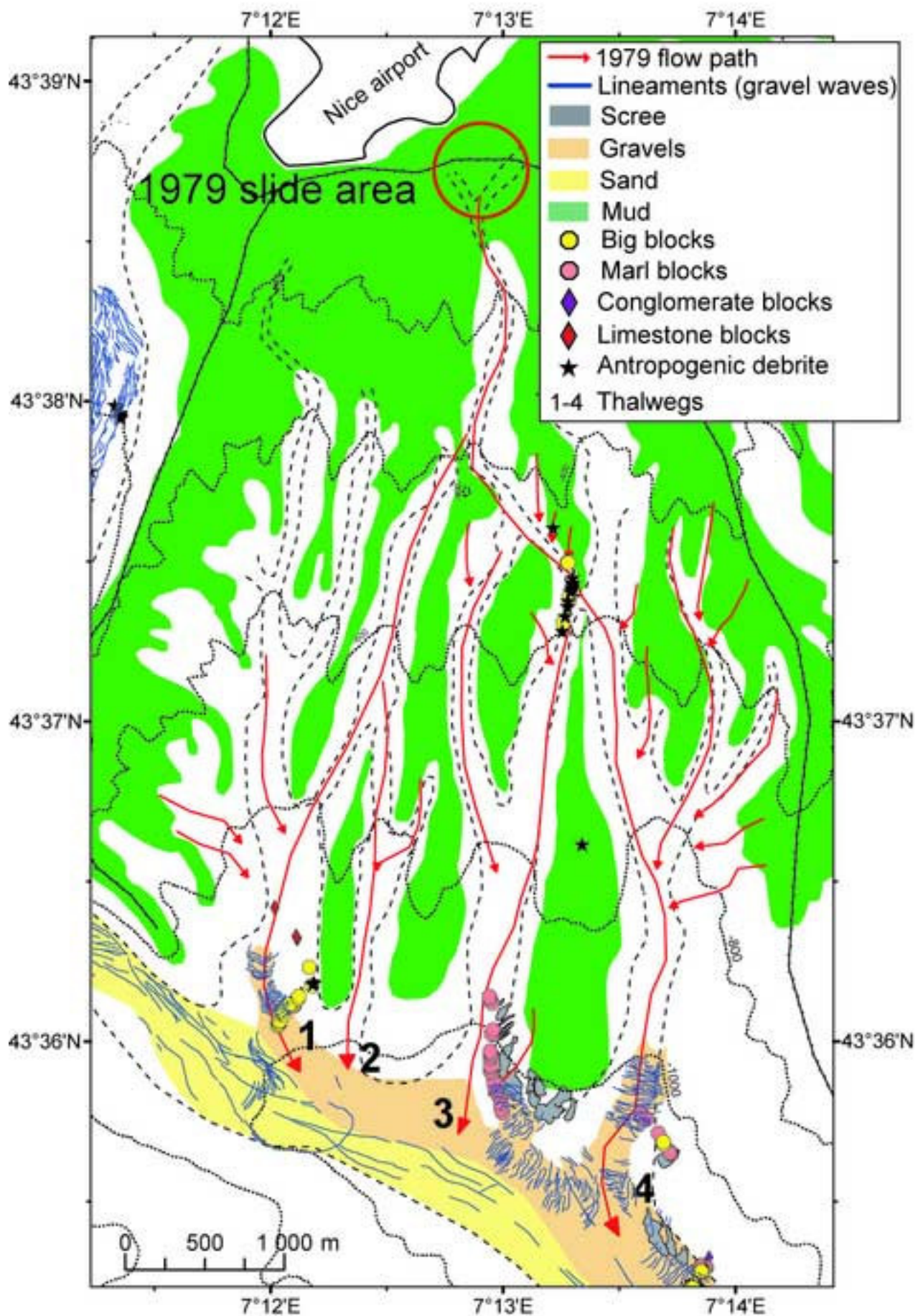
Figure 9

Figure 10
Click here to download high resolution image

Figure 10

(a)

(b)

Figure 13
Click here to download high resolution image

(1)

(a)

sensitive clay

Present seafloor

FOS = 1.45

(b)

Present seafloor

0.105 0.085 0.065 0.045 0.025 0.005

FOS = 1.45

Distance (m)

(2)

sensitive clay

Present seafloor

FOS = 1.3

Present seafloor

0.105 0.085 0.065 0.045 0.025 0.005

FOS = 1.3

Distance (m)
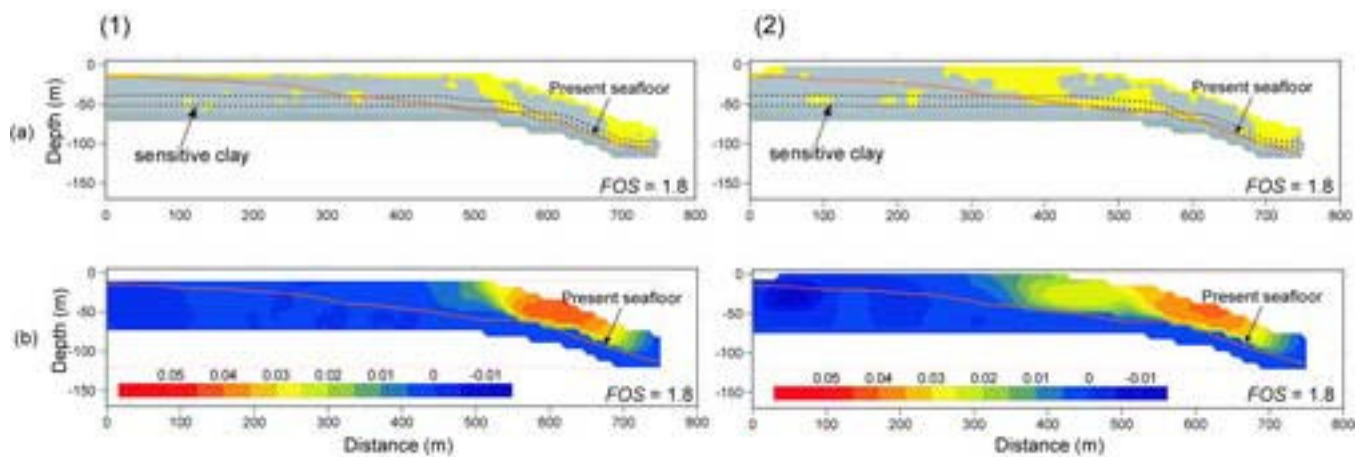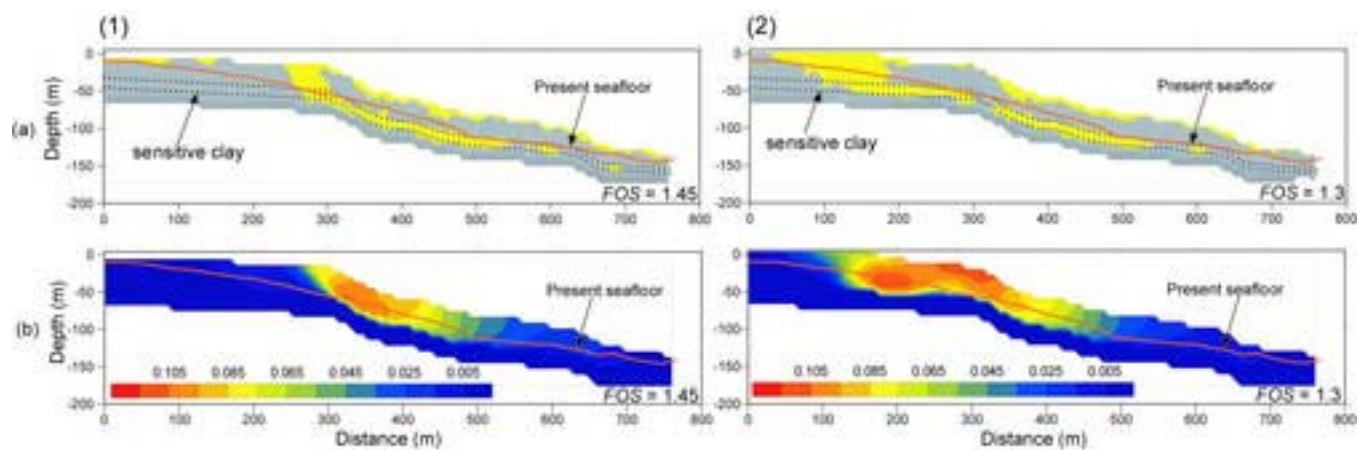
Figure 16
Click here to download high resolution image

(a)

RANGE OF ENGINEERING
INTEREST

Failure

$\ln \dot{\varepsilon}$

GIVEN TIME AFTER START OF CREEP

0

D

(b)

σ

Creep
to failure

Onset of tertiary creep

Creep failure

Critical ?
State Strenght

Initial
stress level

Creep at constant stress

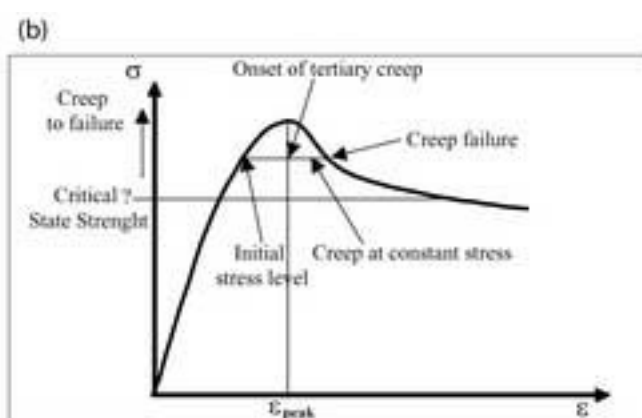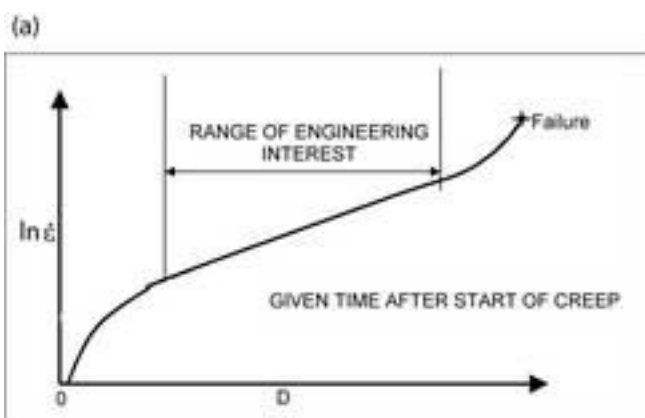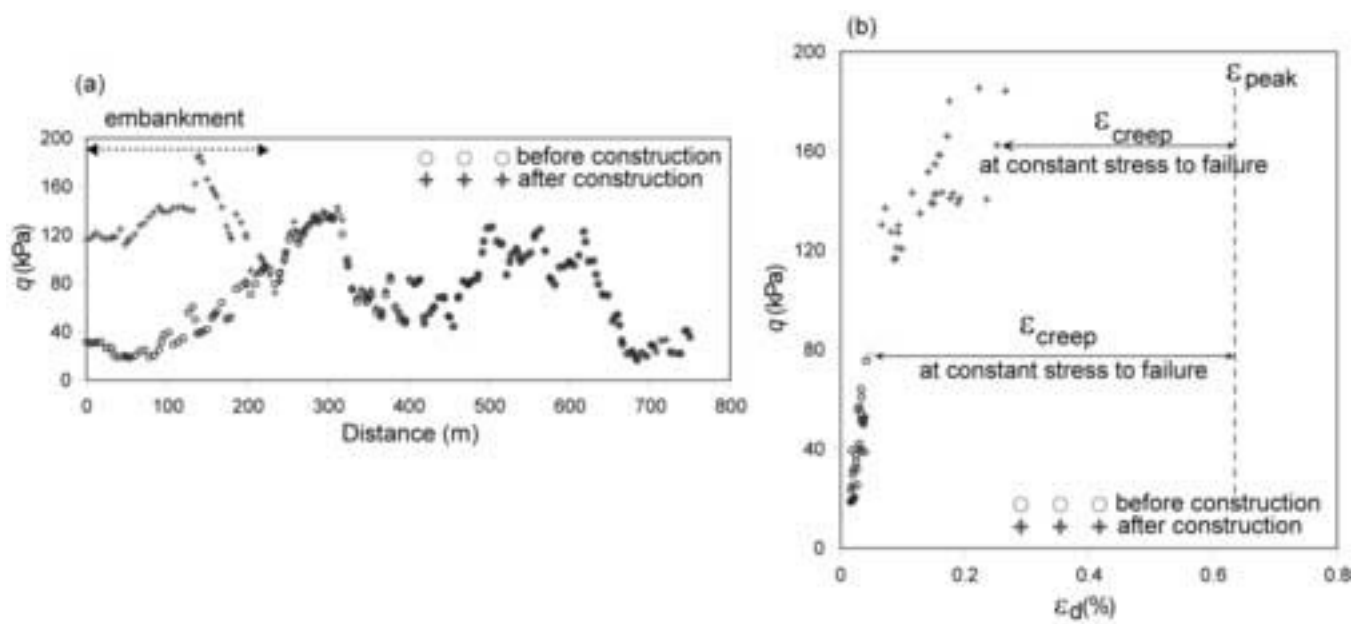ε_{peak}

ε
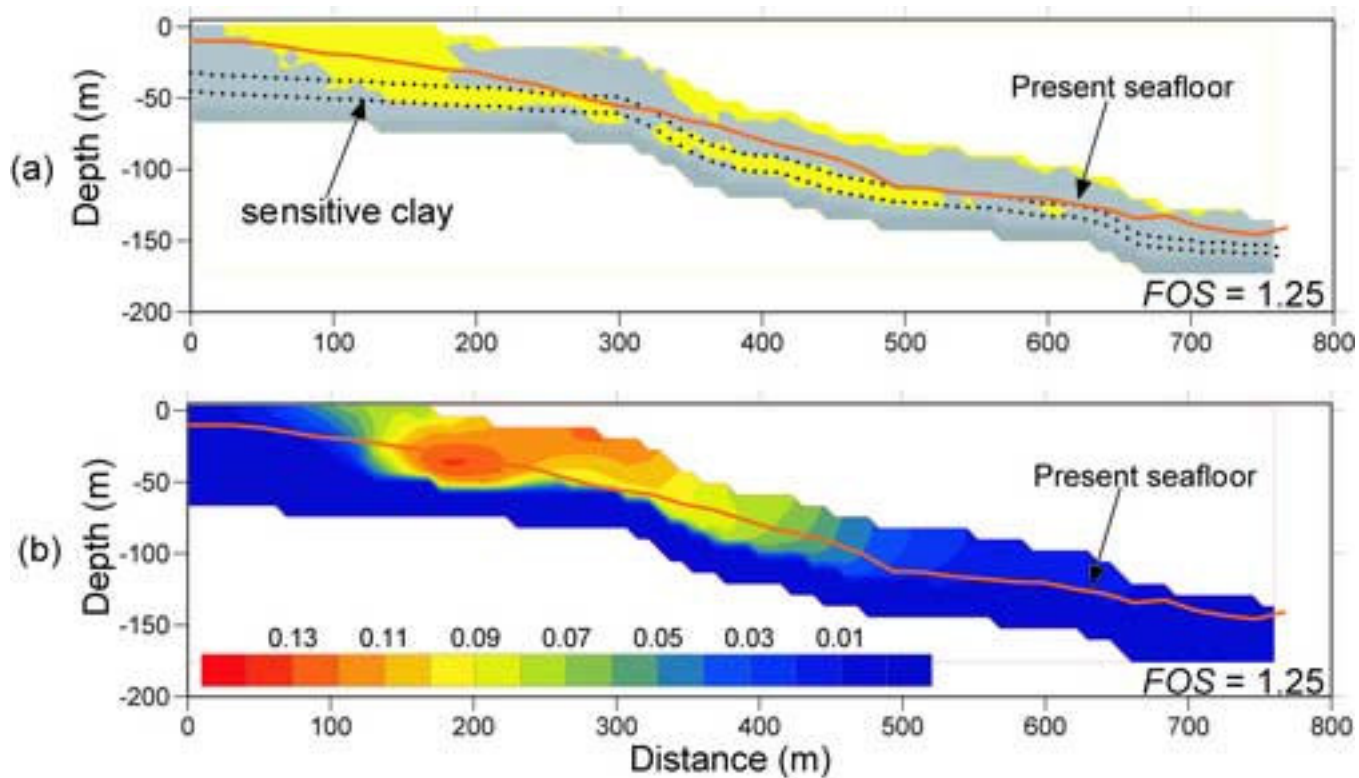
Figure 18
Click here to download high resolution image

Figure 19
Click here to download high resolution image

(a)

Displacement (m)

Factor of Safety

FOS = 1

(b) Depth (m)

Present seafloor

sensitive
clay layer

(c) Depth (m)

Present seafloor

0.09 0.08 0.07 0.06 0.05 0.04 0.03 0.02 0.01 0

Distance (m)
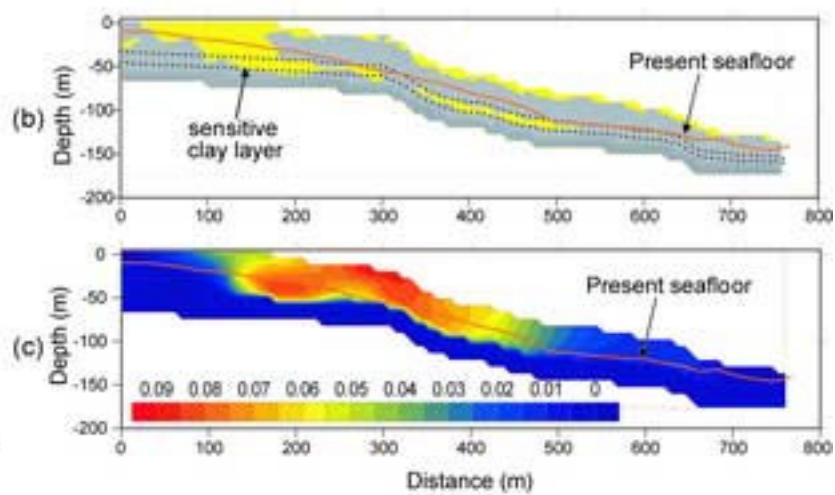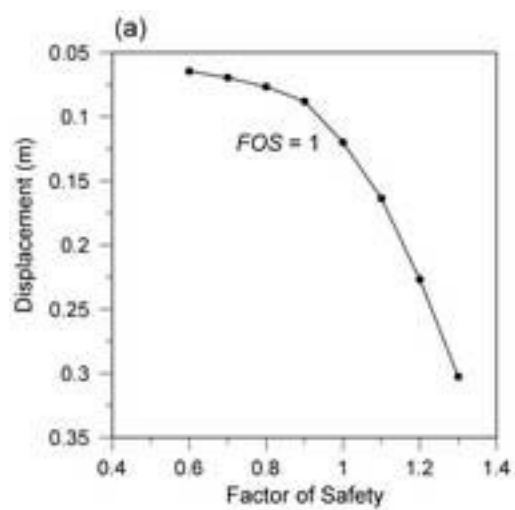
Figure 20
Click here to download high resolution image

(a)

Creeping

high
permeability
sand

high sensitivity

high sensitivity

Fresh water

(b)

Embankment

Creeping

high
permeability
sand

high sensitivity

Softening

high sensitivity

Fresh water

(c)

Embankment

Creeping

high
permeability
sand

high sensitivity

high sensitivity

Increase pore
pressure

Present seabed
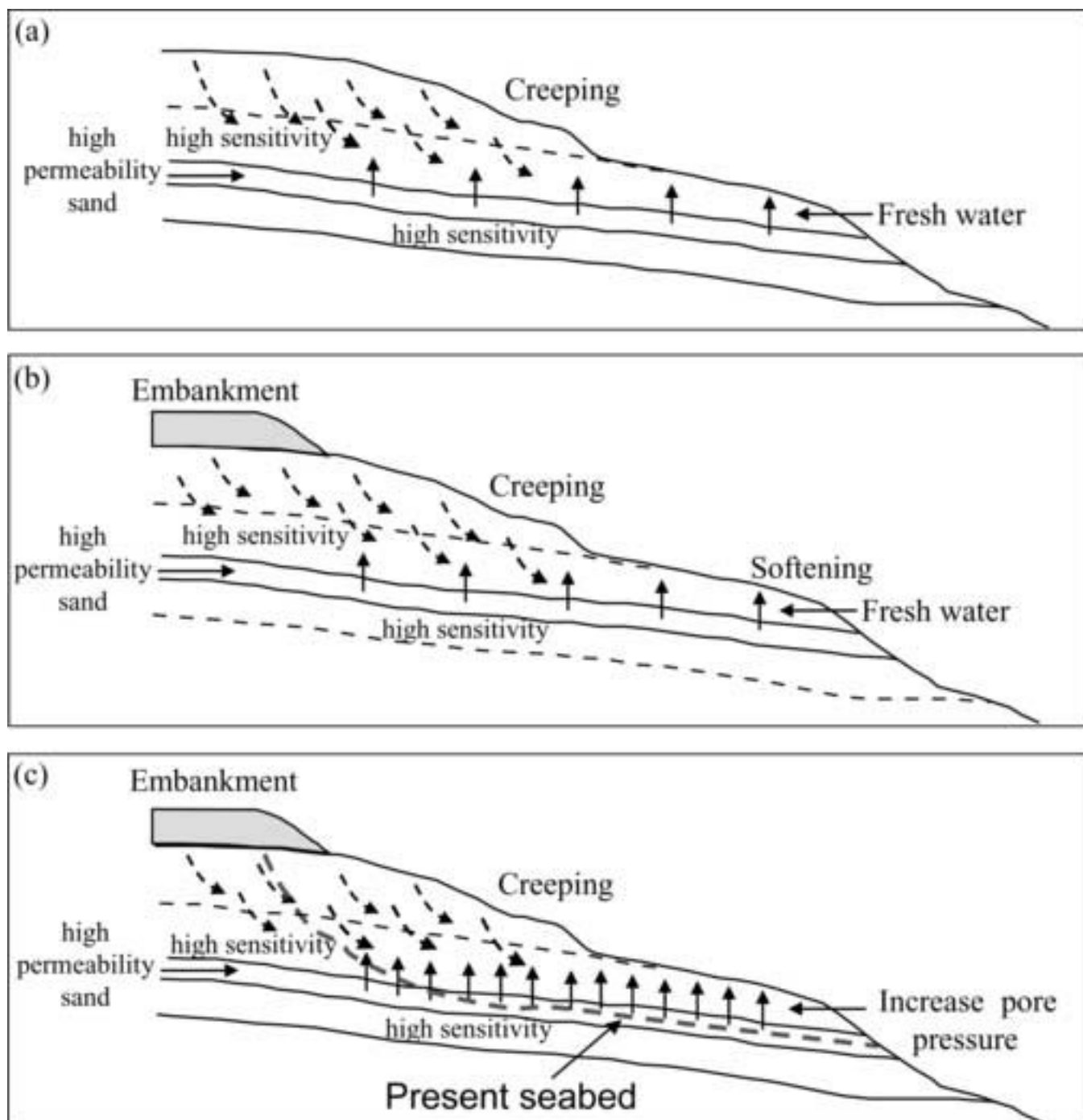
Core	Depth (m)	$\sigma'p$ (kPa)	$\sigma'v$ (kPa)	OCR
KENV2-01	0,14	70,6	1,27	55,6
KENV2-01	0,6	116,2	6,02	19,3
KENV2-01	1,37	155,6	13,88	11,21
KENV2-02	0,91	210	9,92	21,17

TABLE 1

Layer	Lithology (from PZ11)	Thickness (m) (from PZ11)	Su (kPa) (from PZ11)	φ (degrees) (from PZ11)	γ' (KN/m³) (from PZ11)
1	Sand	0,05	0	34	6,5
2	Clay	0,95	67,28	0	6,5
3	Silt	1,35	0	36,9	6,5
4	Clay	1,75	61,89	0	6,5
5	Clay	0,7	59,2	0	5,2
6	Sand	0,3	0	32	5,2
7	Clay	6,36	71,78	0	5,2
8	Sand	0,4	0	33	5,2
9	Silty clay	8,53	70,39	0	7,15
10	Sand	0,5	0	33	7,8
11	Silty clay	5,9	65,26	0	7,93
12	Sensitive clay	12,9	68,62	0	9,1
13	Substratum	8,35	130	0	10,4
14	Substratum	9,45	400	0	10,7

Su: Undrained shear strength

φ: Internal friction angle

γ': Submerged unit weight

TABLE 2

	NW-SE Profile				ENE-WSW Profile	
	Before construction	After construction	Seed's hypothesis	Sensitive clay creep	Before construction	After construction
FOS	1.45	1.3	1.25	1	1.8	1.8

TABLE 3